The refraction of shock waves at a gaseous interface

By ROBERT G. JAHN

Department of Physics, Lehigh University, Bethlehem, Pennsylvania

SUMMARY

A programme of shock tube experiments has been conducted to study the refraction of plane shock waves at interfaces between two gases. Shocks of strength $\xi = 0.85$ (weak) and $\xi = 0.30$ (fairly strong) were allowed to impinge, at various angles of incidence, on interfaces between air/CO_2 and air/CH_4, and the resulting configurations were photographed through a Mach–Zehnder interferometer. From the interferograms, measurements were made of the strengths of the reflected waves, and of the angles of refraction, and the values were compared with the theoretical calculations of Polachek & Seeger (1951). Within the range of parameters for which the refraction model assumed by the theory is applicable—the so-called 'regular refraction' region—the observations were in excellent agreement with the theoretical predictions.

When the study was extended to ranges of the parameters for which the theory is clearly inadequate, a succession of rather complex 'irregular refraction' patterns was observed. Although these configurations were highly interesting qualitatively, each of them involved curved shocks, non-uniform regions of flow, and other less simple processes which discouraged any formal theoretical analysis. On a less rigorous basis, however, it could be shown that these patterns were internally consistent, and that each represented a distortion of a regular refraction process which was reasonable under the prevailing aerodynamic conditions.

Certain observations in these refraction experiments appear to be of some significance outside the specific problem. (i) The sensitivity of strong shock refractions to the values of the specific heat ratio γ for the two gases suggests a possible technique for the measurement of γ and its temperature dependence. (ii) Two of the irregular refraction patterns display a transition process which would be equally appropriate to the onset of the Mach configuration in the shock reflection problem. (iii) Some irregular refractions can be considered as special cases in the problem of the interaction of a shock and a boundary layer.

I. INTRODUCTION

Of the many non-linear phenomena available for physical study, the behaviour of shock waves in gases is one of the neatest and least complex.

Even so, shock wave problems are difficult to treat theoretically, and computations on even the most fundamental shock interactions tend to become involved and somewhat ambiguous. Normally it must fall to direct experiment to clarify the theoretical predictions, and to extend the understanding into regions too complex for mathematical solution. This paper discusses a programme of shock tube experiments which is intended to clarify and supplement the existing theoretical information on one of the most basic shock interactions—the refraction of plane shock waves at an interface between two gases. It is a condensation of a doctoral thesis submitted by the author to the Department of Physics, Palmer Physical Laboratory, Princeton University. Throughout the paper, a dagger (†) is used to indicate specific points discussed in greater detail in the original work, which is available on request from the Princeton University Library.

II. Theory

Theoretical description of this problem has been formulated independently by Taub (1951) and Polachek & Seeger (1951). They assume the same, somewhat idealized model for the refraction process, which is outlined briefly here to introduce the notation and terminology in this paper (see figure 1).

A plane, flat-topped shock I of strength ξ (ξ = pressure ahead/pressure behind) travelling in an ideal (inviscid, with constant specific heat and zero thermal conductivity) gas (1) is incident at some angle α on a plane interface O of another ideal gas (5). Assume that a plane, flat-topped shock T of strength ξ'' is transmitted at an angle α'', and a similar shock RS of strength ξ' is reflected at an angle α'. Assume also that the gas interface passed over by the intersection X is deflected through an angle Δ, and that each of the five angular regions (1) to (5) formed by this configuration is uniform in all its pertinent properties: pressure p, density ρ, temperature T, velocity of sound a, entropy s, and gas flow velocity u. Such a process will be called a 'regular refraction'.

The problem is formulated from the point of view of an observer travelling with the intersection point X. Such an observer sees a certain gas inflow velocity in regions (1) and (5), $u_1 = u_5$. The gas flow u_1 is decelerated and deflected through an angle δ by I, and again decelerated and deflected through δ' by RS. The flow u_5 is deflected through δ'' and decelerated by T. The problem is solved by appplying the Rankine–Hugoniot shock equations, in the form relating change in flow velocity to shock strength, across I, RS, and T, under the boundary requirements that the outflow velocities u_3 and u_4 be parallel (though not necessarily equal), and the exit pressures be the same, that is, under the requirements $\delta + \delta' = \delta'' = \Delta$, and $p_3 = p_4$.

Polachek & Seeger (1951) increased the range of applicability of their refraction model by admitting the possibility that, instead of a shock, the reflection could be a Prandtl–Meyer angular rarefaction wave, centred at X. Such a reflection (hereafter denoted by RR) would accelerate the flow u_2

and deflect it toward, rather than away from the interface. Furthermore, they recognized that any particular gas combination was not necessarily restricted to just one or the other type of reflection, but that reflected shocks might occur for small angles of incidence, and reflected rarefactions for more glancing angles, or vice versa. (The angle of incidence at which such a change takes place we call α_t,—the transition angle.)
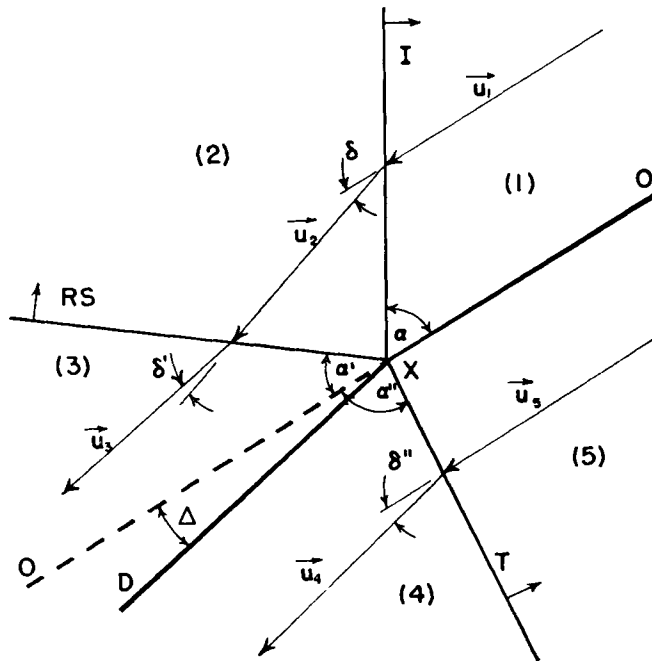

Figure 1. Assumed configuration for the shock refraction process. I = incident shock; RS = reflected shock; T = transmitted shock; α, α', α'' = angles of incidence, reflection, refraction; X = point of intersection of I, RS, and T with interface; OXO = original interface; XD = deflected interface; Δ = angle of deflection of interface; u = gas flow velocity; δ, δ', δ'' = angles of deflection of flow by shocks I, R, T, respectively. Numeral subscripts refer to the 5 angular sectors of the pattern.

Both Taub (1947) and Polachek & Seeger (1951) have carried out extensive numerical calculations, based on their own formulations, of the reflected and refracted wave strengths and angles for various gas combinations, shock strengths, and angles of incidence. In both cases, the automatic calculators can solve the problems only incompletely. For some values of the pertinent parameters they return several solutions; for others, none at all. In the former cases it is necessary to choose one branch of the solutions on the basis of some boundary value criteria, such as the known behaviours in the limits $\xi \to 1$ (acoustic case) and $\alpha \to 0$ (normal incidence). In the latter situations it is presumed that this

2 H 2

idealized model for the refraction process is inadequate to satisfy simul-
taneously all of the aerodynamic requirements, and that some other, more
complex processes must occur physically.

III. DESIGN OF THE EXPERIMENTS

The theoretical approach outlined above was given encouragement by
some early experimental work of Stoner, Woodbridge & Davies (1952),
Bitondo (1950), and the Princeton laboratory, which indicated that a
process quite similar to that assumed by the theory did occur physically.
This process was observed to occur for each gas combination and shock
strength tested, over a range of angles of incidence from normal up to a
certain limiting angle, which depended on ξ and the gas combination.
In the range of α beyond this limiting angle, other more complex inter-
actions, called 'irregular refractions', were observed, which were clearly
incompatible with the simple process assumed by the theory. However,
this early work was largely qualitative, involving shadow photographs and
streak photographs, from which it was possible to measure wave angles,
but not shock strengths or pressure fields directly. It was felt that an
experiment which provided direct measurements of the wave strengths and
pressure distributions throughout the entire refraction field was necessary
if the assumptions and solutions of the theory were to be checked thoroughly
and the complex irregular patterns were to be understood at all.

Of the two sets of calculations that were available, those of Polachek &
Seeger (1951), which included the cases both of reflected shocks and
reflected rarefactions, seemed more appropriate for experimental compari-
son. (Henceforth we refer to these exclusively.) The results of those
computations were presented in the form of graphs of $1/\xi'$ *vs* α and α'' *vs* α
for seven shock strengths and twenty-four gas combinations. These
graphs, largely unpublished, were made available from the Naval Ordnance
Laboratory, by the kind cooperation of Mr L. D. Krider. The experi-
mental work described below was first directed toward a quantitative
appraisal of these regular refraction solutions, and then extended to explore,
qualitatively, the theoretically opaque regions of irregular refraction.

The Princeton laboratory is fortunate to possess a 5-inch Mach–Zehnder
interferometer, with which the gas density in the entire interaction field
can be evaluated. With this equipment available, the experimental problem
resolved itself into the creation of a suitable shock wave refraction process
in the test section of the shock tube. This, in turn, depended primarily
on the accomplishment of a nearly ideal separation of two gases to form a
plane refracting interface there. To date, the only successful means of
gas separation we have found for this experiment has been by some type of
film or membrane. Such a film must be sufficiently strong to withstand
the hydrostatic pressure of the heavier gas, and must be impermeable to
both gases. On the other hand, it must have a sufficiently small mass for
its acceleration by the incident shock not to interfere appreciably with the
refraction process.

Finding a film that satisfies these requirements is the key to the entire experiment. A natural first attempt was to try soap films, which have conventionally been used for similar purposes (cf. especially Stoner's use of soap films for refraction experiments). It quickly appeared, however, that soap films had several inherent disadvantages in this application. (i) They must be drawn in place at the time that they are to be used. (ii) They evaporate, thereby contaminating with water vapour the gases they are separating. With some gases (for example, CO_2) they react chemically. (iii) If used in any position other than horizontal, they drain toward the lower edge and become non-uniform in thickness. (iv) They stretch comparatively easily, and hence tend to bow out under the hydrostatic pressure of the heavier gas, thereby establishing a curved interface. (v) When broken accidentally, or by the incident shock, they splatter the optical flats with soap solution.

After considerable investigation of this film problem, a more suitable gas separation technique was developed using a commercial lacquer film ('Zapon–Aquanite A', a product of the Atlas Powder Company, Wilmington, Delaware). Briefly†, the films are cast on a surface of distilled water, lifted off on stainless steel frames, and allowed to dry. They weigh, when dry, approximately 5 micrograms/cm², and in thickness are a small fraction of one wavelength of visible light. These Zapon films overcome the above disadvantages of the soap films, yet are simpler and more convenient to prepare. They can be made lighter, in total mass, than the soap films that would be needed to hold the same gases over the same size span. It is no exaggeration to say that it was the neatness and manageability of these thin films which made possible an accurate quantitative refraction experiment.

The bulk of the apparatus had to be designed around these all-important films. For example, it was necessary to reduce the effective width of the shock tube test section from 4 in. to 1 in., even though this decreased the optical sensitivity of the experiment, since thereby we could gain a factor of about sixteen in the strength of a film of given thickness. Also, it was necessary to grind narrow slots in the glass windows of the observation section, in order that the edges of the stainless steel frames that held the films could be recessed therein and not obstruct the gas flow in the region of interest.

The apparatus and technique of the experiment can best be visualized by reference to the diagram and photograph shown in figures 2 and 3 (plate 1). The principal piece of special equipment is a shock tube test section H, made of 1-in. dural plate and having internal dimensions 35 in. × 17¼ in. × 1 in. Through the walls of this test section is mounted a cylindrical refraction cell K, which contains the two slotted observation windows R, and suitable valves and seals for introducing and holding the refracting gas. This cell rotates, and with it the interface-forming film J, to permit incidence of the shock wave from any angle from normal to glancing. The lower part of the test section contains a system of gears and shafts which permits a two-directional adjustment of an 18-in. leading plate P. The purpose of this

plate, and a similar but shorter back plate Q, is to present the incident shock to the gas interface in as neat and uncomplicated a manner as possible.
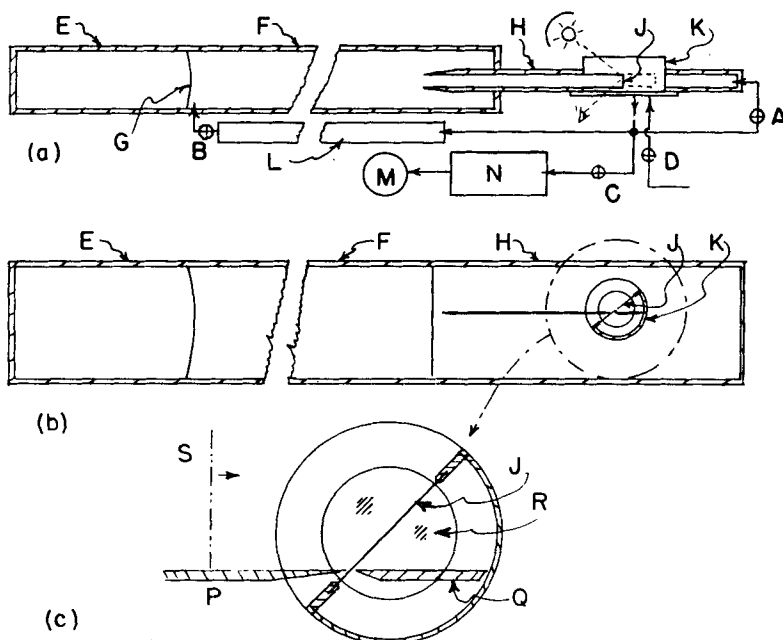

Figure 2. Schematic diagram of shock tube and auxiliary equipment for refraction
experiments : (a) top view; (b) side view; (c) enlargement of test cell. *A, B,
C*, and *D* are valves controlling the flow of gases to and from the rear half
of the refraction cell; *E* = shock tube chamber; *F* = shock tube channel;
G = plastic diaphragm; *H* = test section; *J* = interface-forming film;
K = refraction cell; *L* = exhaust tank; *M* = mechanical pump; *N* = low-
pressure reservoir; *P* = leading plate; *Q* = back plate; *R* = slotted glass
windows; *S* = shock front advancing on refraction cell.

The technique actually followed in these experiments might best be illustrated in the form of a step by step recipe.

(i) The films are cast on their frames and allowed to dry.

(ii) The entire shock tube is completely evacuated, and the appropriate pressure is set in the high pressure chamber E. The channel F and test section H are then returned to atmospheric pressure.

(iii) The Zapon film, held on the stainless steel frame on which it was cast, is set into place between the slotted windows J. The refraction cell K is inserted into the test section at the desired angle and sealed to it. (Note that it is necessary to carry out steps (ii) and (iii) in this order. The thin Zapon films are so delicate that, if they were present inside the shock tube while the high pressure was being set in the chamber, they would be broken by the minute pressure pulses emitted by the plastic diaphragm G as it stretches into position.)

(iv) The leading plate P and back plate Q are adjusted until they nearly touch the film interface at its most forward point.

(v) With valves A and B open, the shock tube channel and test section are evacuated again, quite slowly, until p_1 and p_5 are equal to the desired downstream pressure. (The connection through valve A equalizes the pressures on either side of the film during the pumping process more readily than the longer connection *via* valve B.)

(vi) With valve A closed and B open, the refracting gas is now introduced very slowly into the rear of the cell *via* needle valve D, replacing the air there which exhausts into a large tank L mounted by the side of the shock tube. The other end of this exhaust tank is directly connected to the shock tube channel, thereby automatically maintaining $p_1 = p_5$. The tank is sufficiently large, and contains baffles so arranged that practically none of the exhaust gas ever drifts into the shock tube. Since the flow path of this arrangement is long compared with the size of the various orifices involved in the plumbing, p_5 tends to remain slightly higher than p_1 for any reasonable rate of flow. To compensate for this, needle valve C, connecting an evacuated reservoir (N) with the exhaust line, provides a further fine adjustment on p_5.

An external indicator of the pressure difference across the film, of the extreme delicacy needed to protect the films throughout the above process, might be difficult to arrange. But fortunately, since the interior of the refraction cell is visible through the windows, the films themselves can serve as pressure indicators. Normally, they respond to a pressure difference by a slight elastic bowing into the lower pressure region before they break. By careful observation of such distortions it is usually possible to control the gas flows sufficiently accurately to avoid a rupture. In practice, the operator, holding needle valve D in one hand and C in the other, watches the oblique reflection of a circular light source from the front face of the film. As the film bows slightly in or out under an incipient pressure difference, the reflected image becomes elliptical in one direction or the other. Keeping this reflected image as nearly circular as possible, the operator gradually opens the two valves until a reasonable flow of gas is established.

(vii) After the gas has been flowing thus through the rear half of the cell for five or ten minutes, the shock tube is fired, sending a plane, flat-topped shock wave down the tube toward the test section. Two sharp plates extending up the tube from the test section literally slice out of this shock front a 1-in. strip, which then travels over the leading plate and is presented to the 5 in. × 1 in. gas interface in the refraction cell.

Spark photographs of parallel fringe interferograms of the resulting refraction process are taken through the Mach–Zehnder interferometer. These interferograms are analysed by the standard superposition method (see Bleakney & Griffith 1954) to determine the density field, from which the shock strengths and pressure distributions can be computed.

Measurements of the wave angles can also be taken directly from the interferograms.

White light interferograms are obtained simultaneously, which aid in determining the integral fringe shift across the various density discontinuities. Two light screens record the velocity of the incident shock wave as it travels down the tube and thereby offer a double check on its strength.

There are three significant restrictions on the ideality of this experiment: the effect of the finite mass of the film, which will be discussed later; the inability to obtain completely pure gas in the refracting cell, which must be considered in the evaluation of the data†; and one other, which arises as an unavoidable consequence of the physical boundaries at which the observed refraction process begins. Nowhere in the theoretical treatment is there considered the practical limiting condition that the outflow from the reflected and transmitted waves must be supersonic in their respective gases with respect to the intersection point if regions (3) and (4) are to retain portions undisturbed by foreign signals. That is, regardless of the apparatus, the 'corner' at which the refraction process starts will radiate signals which travel out into the flow with the local sound velocity. For sufficiently glancing angles, such corner signals can 'catch' the intersection point, distort the reflected or transmitted waves, or both, and destroy the uniformity of all of regions (3) and (4), thereby violating the theoretical assumptions. This effect imposes on the regular refraction process two limiting angles†, α_{sr} and α_{st}, beyond which the observations cannot be expected to agree with the theoretical predictions. Fortunately these angles usually occur near the end of the theoretical regular refraction region, and therefore this situation does not require serious consideration until one wishes to study the irregular refraction configurations (see § VI).

Five dependent quantities are available for measurement from the interferograms obtained by the technique outlined above: ξ', ξ'', α', α'', and Δ. Of these, ξ' and α'' are the most significant to study. ξ', the strength of the reflected wave, is the most sensitive index to the refraction process, changing by large fractions of itself for comparatively small changes in the experimental conditions; and although the reflected waves are always quite weak, and the fringe shifts across them correspondingly small, the interferometric technique permits sufficiently accurate measurement of ξ' to make it an ideal quantity to study. The angle of refraction α'', though less sensitive to the parameters, is always sharply defined on the interferograms.

The remaining three quantities cannot be obtained with comparable accuracy. The evaluation of the refracted shock strength ξ'' is rather sensitive to the optical properties, and hence to the purity of the refracting gas, which varies appreciably from shot to shot. The reflected wave is so weak that the angle α' it makes with the interface is not measurable with adequate precision. (This measurement is particularly difficult when the reflection is a rarefaction fan.) Finally, the measurement of the deflection angle Δ is inaccurate because the deflected interface is rather broad and indistinctly defined on the interferograms, and because this region of the

pattern is complicated by spurious signals from the corner. Fortunately, it is also true that the angles α' and Δ are less sensitive indices to the refraction pattern than the other variables†.

Therefore, in these experiments we concentrated on the measurement of ξ' and α''. Since one of these pertains to the reflection and one to the refraction, accurate evaluation of these two can check the entire regular refraction solution. In the analysis presented in the following sections, our approach is to superimpose experimental data of ξ' and α corrected for conditional variations, on the theoretical curves of $1/\xi'$ *vs* α for the appropriate shock strength and gases. We also compare theoretical curves of α'' *vs* α with the experimental values and show that these are less sensitive to the conditions of the problem. In a few cases, we include a few spot checks on α', ξ'', and Δ to preclude any major deviation from the assumed configuration from passing unnoticed.

Once the feasibility of the technique outlined above was established by a few preliminary tests, it became necessary to select the range of initial conditions that a systematic set of experiments should cover. In this experiment, as in almost any practical refraction situation, the five independent variables of the theory (ξ, α, γ_1, γ_5, a_1/a_5) are embodied in three physical conditions, ξ, α, and the gas combination. Of the many combinations of these conditions which could be investigated in the shock tube, it was desirable to select those cases that could be handled most simply, yet still provide a truly representative check of the idealized theory. In the experiments described below, study was made of the refraction of shocks of strength $\xi = 0.85$ and $\xi = 0.30$ incident at angles from $\alpha = 0$ to glancing, on interfaces between air and carbon dioxide, and air and methane (hereafter denoted by air/CO_2 and air/CH_4). The reasoning behind these choices can only be outlined briefly here†.

The theory predicts two distinct classes of solutions, those which involve a reflected shock at $\alpha = 0$, and those which involve a reflected rarefaction at $\alpha = 0$, depending on the condition

$$\frac{\Gamma_5}{\Gamma_1} = \left\{\frac{\gamma_5[(\gamma_5+1)+(\gamma_5-1)\xi]}{\gamma_1[(\gamma_1+1)+(\gamma_1-1)\xi]}\right\}^{1/2} \frac{a_1}{a_5} \gtrless 1.$$

More detailed study of the way in which the gas properties enter into the problem, and of the results of the computations for many varied gas combinations, indicates that, beyond this broad distinction, there is no further significant subdivision of the solution types with respect to gas combinations.

In other words, we can reasonably expect that one representative gas combination from each of the two major classes will adequately simulate the effect of any possible arrangement of the conditions ξ, α, a_1/a_5.

An obvious simplification in the experiment is gained if we choose the gas (1), which in our arrangement must fill the entire shock tube channel, to be air. For the refracting gases (5), other than the requirement that one be 'faster' and one 'slower' than air, the only obvious properties to consider

are their manageability, index of refraction, and the ratio of their sound speed to that of air. In preliminary experiments, refracting gases which were considerably different from air, such as helium and freon, were tried on the theory that the magnitude of the refraction effects would be largest for the most dissimilar combinations. However, the large density differences involved required rather heavy films to withstand the hydrostatic pressures. Also, the large differences in index of refraction made it impossible to obtain good optical fringes over the entire field of both gases. In the long run, it was found best to study two less severe gas combinations, air/CH_4 and air/CO_2. Although the refraction effects are somewhat less pronounced for these cases, the increased precision with which the experiment can be performed more than compensates for this, and a more accurate check on the theory can be made.

The shock strengths $\xi = 0.85$ and 0.30 were chosen, under considerations of operating convenience and pressure limitations of the shock tube, to provide the most reasonable check on the ξ-dependence of the refraction theory†.

The specific details of these experiments and the results obtained from them are described in the remaining three sections of the paper. § IV covers the weak shock experiments, and their results in the regular refraction regions. § V presents the strong shock, regular refraction experiments. In § VI we conclude with a description and brief analysis of the many curious patterns observed in the irregular refraction regions at both shock strengths and for both gas combinations.

IV. EXPERIMENT 1 : THE REGULAR REFRACTION OF WEAK SHOCKS

The first experiment studied the refraction of shocks of strength $\xi = 0.85$ at interfaces between air/CO_2 and air/CH_4 for the dual purpose of testing the technique and apparatus outlined above, and of checking the regular refraction solutions at this shock strength. To accomplish this, refraction interferograms, samples of which are shown in figure 4 (plate 2), were taken in the manner described in § III. From these, measurements were made of reflected wave strengths, angles of refraction, and pressure distributions throughout the interaction field in sufficient quantitative detail to permit reasonable comparison with the appropriate theoretical computations.

Unfortunately, the numerical solutions computed by Polachek & Seeger (1951) involve approximate values for the pertinent gas constants. Specifically, they have assumed that the ratio of specific heats, γ, for both CH_4 and CO_2 is exactly $\frac{4}{3}$, and have rounded off the air/CH_4 and air/CO_2 sound speed ratios to convenient decimals. Before attempting any experimental comparison with their results, therefore, it was necessary to adjust their solutions by using more realistic values for the gas properties. Since these are rather small adjustments, it is adequate to evaluate them by approximate methods. For example, we chose to find the corrections at a few convenient special angles, such as $\alpha = 0$, α_t, α_e, where the computations are simpler, and then to interpolate the remainder of the solutions graphically†.

The conditions of the experiments could not be held sufficiently close even to these more realistic theoretical assumptions to permit immediate comparison of the results. Each observation had first to be adjusted for the experimental deviations from ideality mentioned in § III.

(i) The theoretical curve is based on $\xi = 0.85$. The shock strengths actually used differ by as much as 0.025 from this value. The normalization was handled by cross-plotting graphs of $1/\xi'$ vs ξ for various values of α from the theoretical graphs of $1/\xi'$ vs α for various values of ξ. Taking the slope of the former at the point $\xi = 0.85$ yields a function of α which, when multiplied by the deviation of the experimental value of ξ from 0.85, is just the correction desired.

(ii) Any incompleteness in the gas replacement process resulted in an impurity of the refracting gas and a consequent discrepancy from the values of γ_5 and a_1/a_5 assumed by the theory. The degree of this impurity was measured from a 'blank' interferogram, taken just before the shock tube was fired. The fringe difference across the boundary could be computed from the known index of refraction for the pure gas, and any discrepancy between this difference and that measured on the 'blank' could be used to determine the relative impurity. With this measure of the efficiency of the replacement process, and knowing the composition of the bottled gas, it was then possible to calculate a new γ_5 and a_5 for the impure refracting gas; and from these, corrections to the experimental observations could be made†.

(iii) The effect of the finite mass of the interface-forming film on the refraction configuration had to be checked experimentally. For this particular case, study was made of the density fields resulting from the normal incidence of shocks on films of various thicknesses, with air on both sides. The effect of films even five times more massive than those regularly separating the gases was found to be surprisingly small. Although sharp pulses were reflected from the films, their effective strength, that is, the ratio of the pressure before and after the pulse, was never larger than the 0.001 uncertainty with which the pressure ratio could be measured.

It is conceivable that some other complications could arise from this cause for gas combinations other than air/air and at angles other than $\alpha = 0$. Isolated tests were made at other such conditions, the net result of which was to support the assumption that in neglecting the mass of the film the error introduced was not greater than the uncertainty in the interferometric measurement of $1/\xi'$†. Actually, in the preparation of the data, account was taken of the almost trivial correction suggested by extrapolating the film test results to zero thickness.

In considering the results of this experiment, it is first to be emphasized that the qualitative nature of the interferograms taken in the regular refraction regions agrees closely with the assumptions of the theory. Namely, within the limits of the observation, each pattern is composed of an incident, reflected, and refracted wave, which are radially straight for a finite distance

from the point of intersection with the interface, and between which are regions of uniform pressure.   In no case has any evidence been seen of other signals, either continuous or sharp (except, of course, the corner signals mentioned previously) or of any non-uniformity in the angular regions.

The quantitative results may best be seen in figures 5 and 6.   In figure 5 are plotted the observed values of $1/\xi'$ and α.   The dotted curves of $1/\xi'$ *vs* α represent the original solutions of Polachek & Seeger (1951).   The solid curves are those same solutions, corrected by the use of more realistic gas
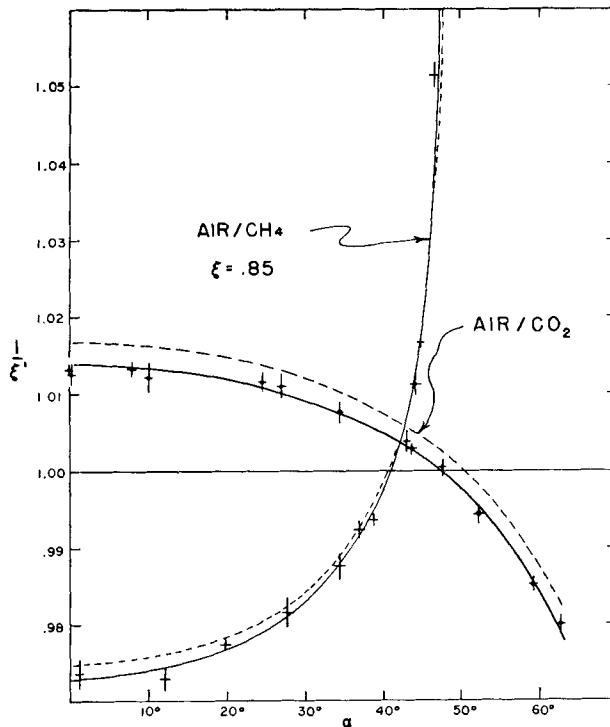
Figure 5. Experimental values of reflected wave strength ξ' superimposed on theoretical predictions, for air/CO_2 and air/CH_4 with $\xi = 0.85$.   Dotted curves represent original Polachek & Seeger (1951) solutions.   Solid curves represent the same solutions, adjusted for realistic gases.

constants.   The experimental points themselves have been individually corrected for variation in incident shock strength, gas purity, and film mass, wherever appropriate.   The error boxes reflect the ability to evaluate $1/\xi'$ from the interferograms with an accuracy of from ± 0.0005 to ± 0.0020, dependent on the particular interferogram.

Also available for comparison with the theory are the experimental values of α'' and α.   In figure 6 the dotted lines of α'' *vs* α represent the original calculated solutions at $\xi = 0.85$; the solid lines are those solutions

corrected as above. The experimental points that are superimposed on them (error boxes are $\pm 0.5°$) have again been corrected for gas impurity, but not for their variations in incident shock strength, since small changes in ξ caused no observable differences in α''. As evidence of this insensitivity, these graphs also show (dashed lines) the computed solutions for a much stronger shock, $\xi = 0.30$. The curve for $\xi = 1.00$, when plotted, could barely be distinguished from that for $\xi = 0.85$.
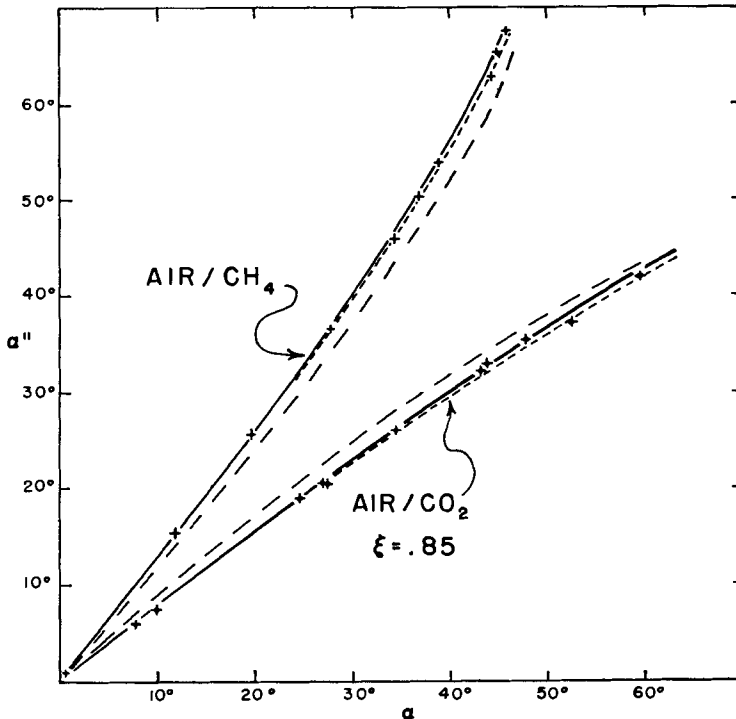

Figure 6. Experimental values of α'' superimposed on theoretical predictions, for air/CO_2 and air/CH_4 with $\xi = 0.85$. For explanation of dotted and solid curves, see figure 5. Dashed curves represent theoretical solutions for $\xi = 0.30$.

A few spot checks were made on the other three measurable quantities, ξ'', α', and Δ. These quantities were not studied so thoroughly as ξ' and α'', and in no case was any attempt made to correct the data for variations in the experimental conditions, or to adjust the computations for more realistic gas combinations. Rather, these measurements, a few samples of which are shown in tables 1 and 2, served merely as a reassurance that no major deviations from the theory were being overlooked by restricting the study of these quantities.

α deg.	α' theo. deg.	α' exp. deg.	Δ theo. deg.	Δ exp. deg.
		Air/CO_2		
0	0	0	0	0
10	8·5	8·3	1·1	1·1
30	26·7	27·6	2·7	2·9
50	48·0	47·2	—	—
		Air/CH_4		
0	0	0	0	0
10	8 5	8·8	1·1	1·2
30	27·7	26·8	2·7	3·0
50	48·0	48·9	—	—

Table 1. Rough spot checks of α' and Δ.

α deg.	ξ'' theo. ($= \xi\xi'$)	ξ'' exp.
	Air/CO_2	
34·5	0·854	0·851
52·5	0·858	0·859
	Air/CH_4	
12·0	0·876	0·878
46·5	0·850	0·851

Table 2. Rough spot checks of ξ''.

V. EXPERIMENT 2 : THE REGULAR REFRACTION OF STRONG SHOCKS

The interferograms obtained of the stronger shock refraction patterns, a few samples of which appear in figure 7 (plate 3), appear much the same as those taken of the weaker shock case.   There have been, of course, certain quantitative changes in the various parameters, notably the increase in strength of each of the three signals, and the change in relative sizes of the angles of the configuration.   The deflection of the interface, Δ, for example,

is uniformly larger, in accordance with the higher flow velocity set up by the stronger incident shock. Similarly, the compounding of this higher flow velocity with the relative velocity of the reflected wave has tended to increase α' for those cases where $\alpha + \alpha' > 90°$ and to decrease α' for those cases where $\alpha + \alpha' < 90°$ (i.e. the flow 'blows back' the reflected wave). Also, the angle of refraction α'' now assumes a value closer to α for both the 'slow/fast' and 'fast/slow' cases, for all $\alpha < \alpha_t$[†].

An interesting feature is exhibited in the white light interferograms, figures 7c and 7d (plate 3). The reflected shock from the air/CO_2 interface at $\alpha = 0$ (figure 7c) is quite sharp and flat-topped. However, the reflected rarefaction from the air/CH_4 interface (figure 7d) has already spread out considerably. Its trailing edge is actually behind the original interface position. Also note that the leading edge of this rarefaction is preceded by a slight compression bump, due presumably to the finite mass of the film.

All of the interferograms obtained in the regular region at this shock strength exhibit excellent radial straightness of the signals, and uniformity of density and pressure within each of the five angular segments, thereby displaying again a close correspondence between the experiment and the theoretical problem.

Air/CO_2	α'' deg.	ξ	$1/\xi'$
Measured value	$39 \cdot 0 \pm 1 \cdot 0$	$0 \cdot 305$	$1 \cdot 0769$
Correction for 9% impurity of CO_2	$+0 \cdot 4$	—	$+0 \cdot 0078$
Correction to make results relate to $\xi = 0 \cdot 300$	—	$-0 \cdot 005$	$+0 \cdot 0016$
Corrected value	$39 \cdot 4$	$0 \cdot 300$	$1 \cdot 0863$

Table 3. Typical sample of corrections applied to measured values of $1/\xi'$ and α''.

Measurements of $1/\xi'$ and α'' were extracted from the interferograms just as before. Again, certain corrections needed to be made before the observed values could be compared with the theoretical calculations. The adjustment of the Polachek & Seeger (1951) solutions for the realistic gas constants was repeated as above. The corrections of the experimental values for the mass effect, the purity of the refracting gas and variation in incident shock strength also proceeded as described for the weak shock case[†]. As an illustration of the relative importance of the various corrections for a strong shock experiment, table 3 shows a breakdown of the computations for one typical pattern.

In evaluating the results of these experiments it is well to bear in mind that the optical sensitivity of the measurements was considerably reduced

by the necessary use of a low p_1.   Assuming that it is possible to measure an interferogram to $\pm 0{\cdot}03$ fringes, $1/\xi$ could be determined to $\pm 0{\cdot}015$ and $1/\xi'$ to $\pm 0{\cdot}006$.   Considering the other uncertainties of the experiment, the error limits for $1/\xi'$ range from $\pm 0{\cdot}006$ to $\pm 0{\cdot}009$.   The angle α'' could normally be determined to $\pm 1{\cdot}0°$, except in a few cases where the corrections were sufficiently large or uncertain to warrant $\pm 2{\cdot}0°$ limits.

Despite this decrease in precision, the results, plotted in figures 8, 9, and 10, show that the experiment is still sufficiently sensitive to trace out a curve of agreement with the corrected Polachek & Seeger computations.
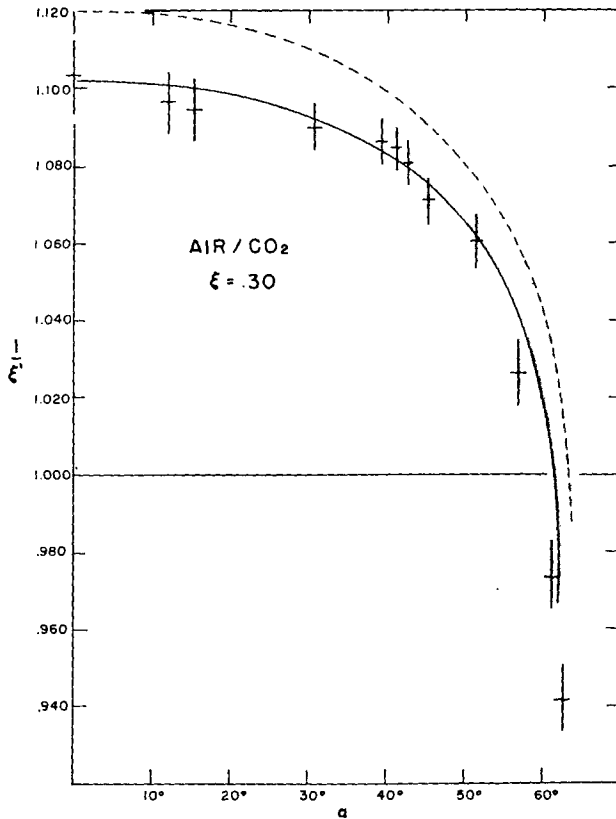
Figure 8. Experimental values of $1/\xi'$ superimposed on theoretical predictions, for air/CO_2 with $\xi = 0{\cdot}30$.   For explanation of dotted and solid curves, see figure 5.

In particular it is interesting to note that the experiment is again capable of choosing between the theoretical curves for the realistic and idealized gases, even though the values of γ and the sound speeds were changed only by 2% or 3%.   Consideration of the sensitivity of the experiment to changes in γ suggests the possibility of designing a more appropriate version of the
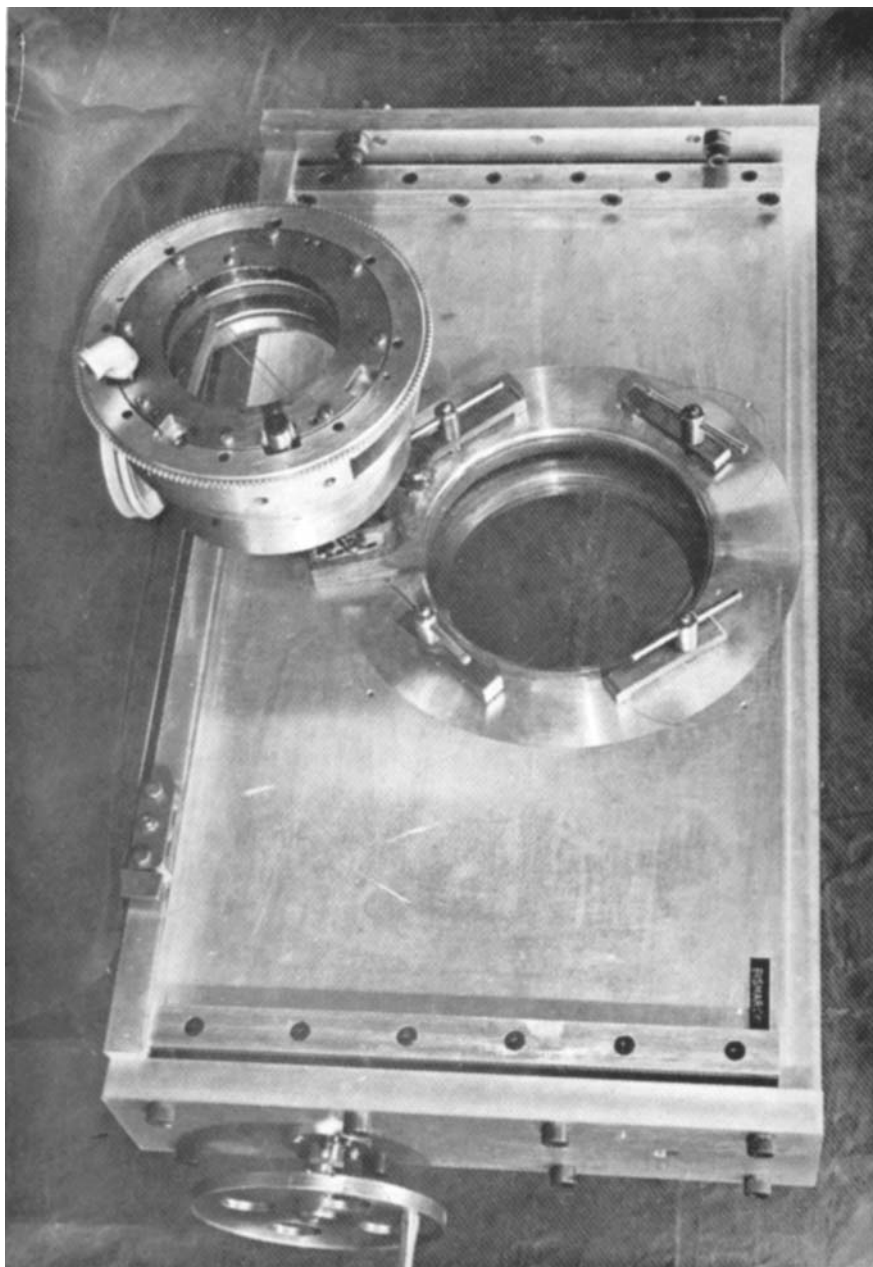
Figure 3. Refraction test section, with rotatable cell removed.
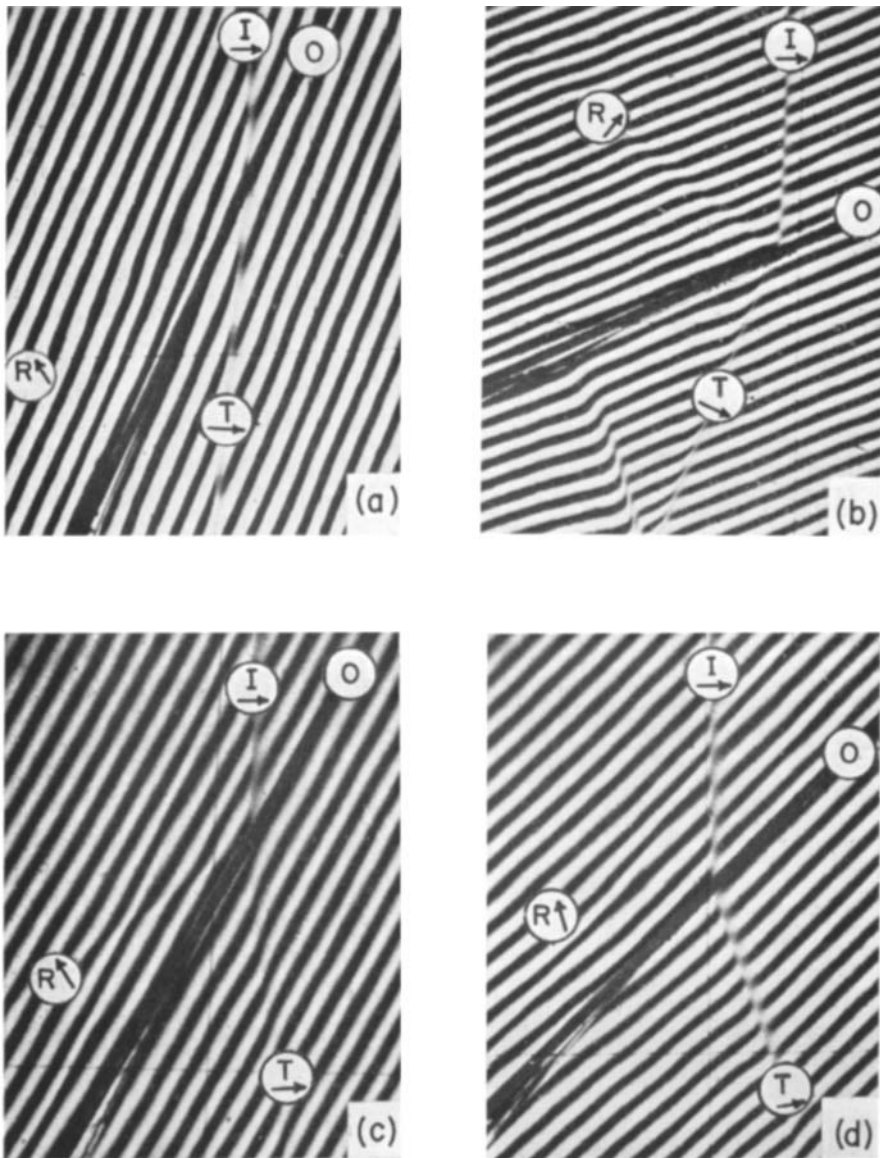
Figure 4. Refraction interferograms for shock strength $\xi = 0.85$: (a) air/CO_2, $\alpha = 25°$ (reflected shock); (b) air/CO_2, $\alpha = 63°$ (reflected rarefaction); (c) air/CH_4, $\alpha = 27°$ (reflected rarefaction); (d) air/CH_4, $\alpha = 45°$ (reflected shock). I, R, T = incident, reflected, and transmitted waves; O = original interface; arrows indicate directions in which I, R, and T are travelling. Fringes shift toward lower right for increase in pressure.
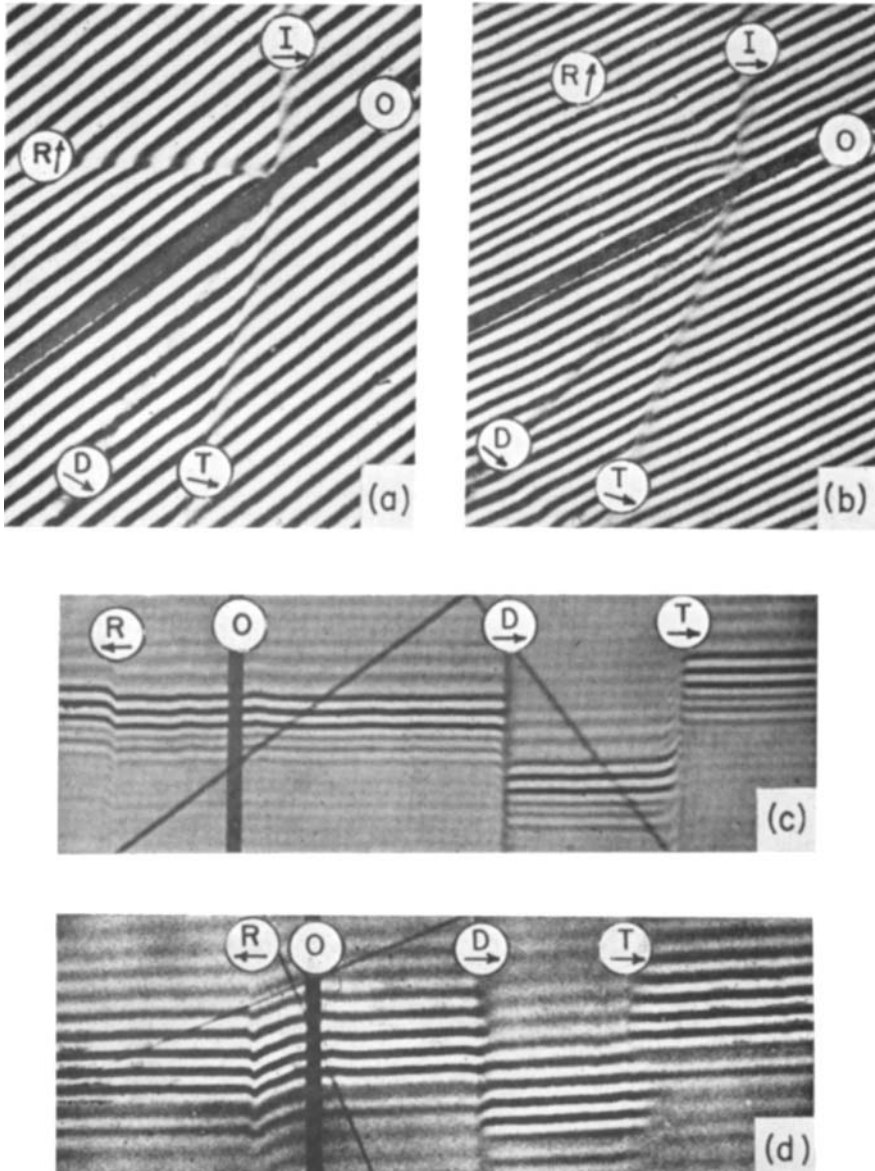
Figure 7. Refraction interferograms for $\xi = 0 \cdot 30$: (a) air/CO_2, $\alpha = 53°$ (reflected shock); (b) air/CO_2, $\alpha = 63°$ (reflected rarefaction); (c) air/CO_2, $\alpha = 0°$ (reflected shock); (d) air/CH_4, $\alpha = 0°$ (reflected rarefaction). I, R, T = incident, reflected, and transmitted waves; O = original interface; D = deflected interface; arrows indicate directions in which waves are travelling. Fringes shift down for increase in pressure.
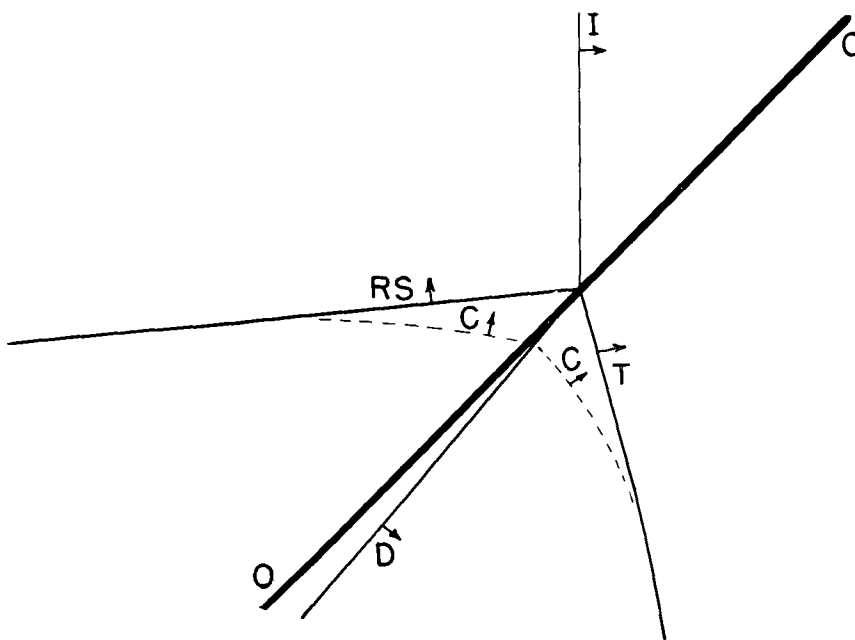
Figure 14 (a). Air/CH$_4$, regular refraction. (I, RS, T = incident, reflected, transmitted shocks; O, D = original, deflected interfaces; C = corner signal.)
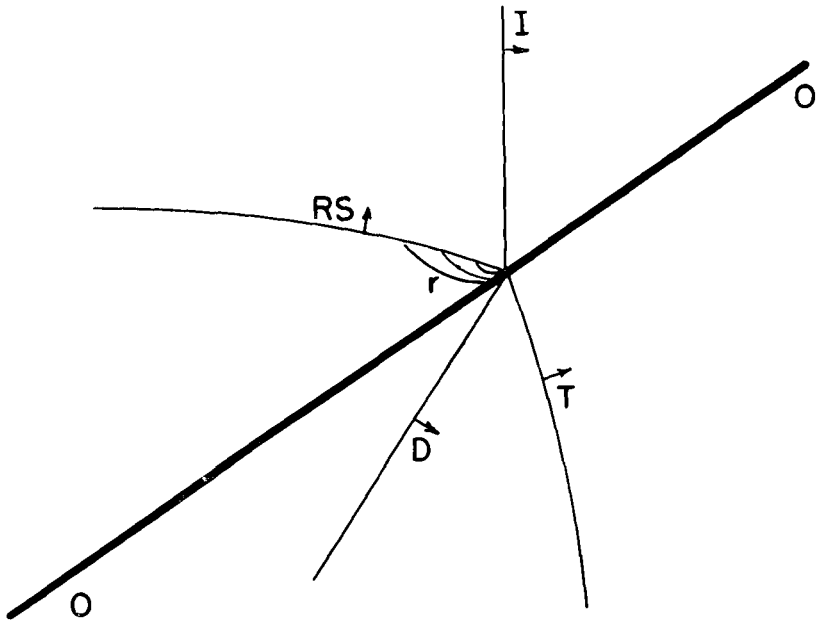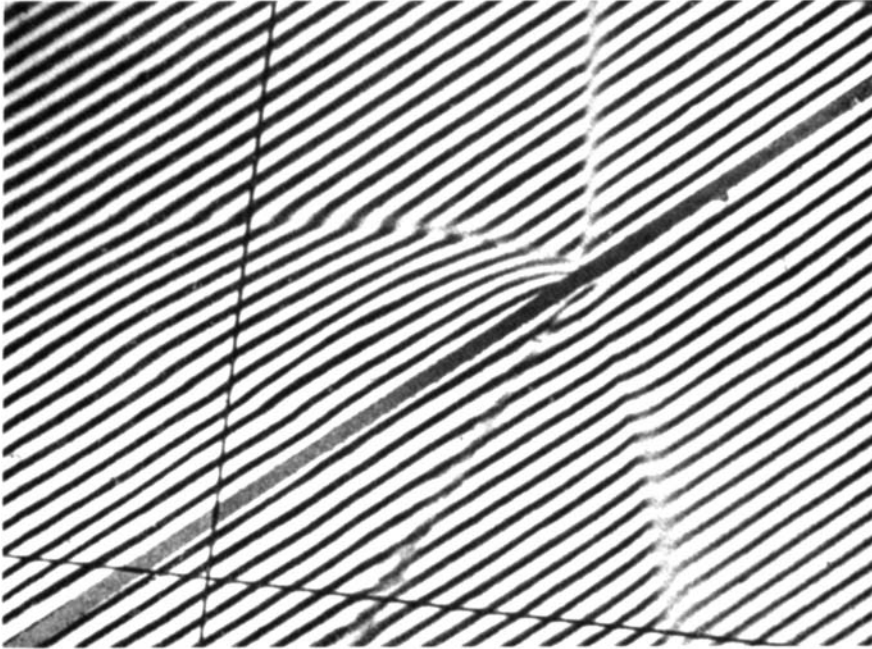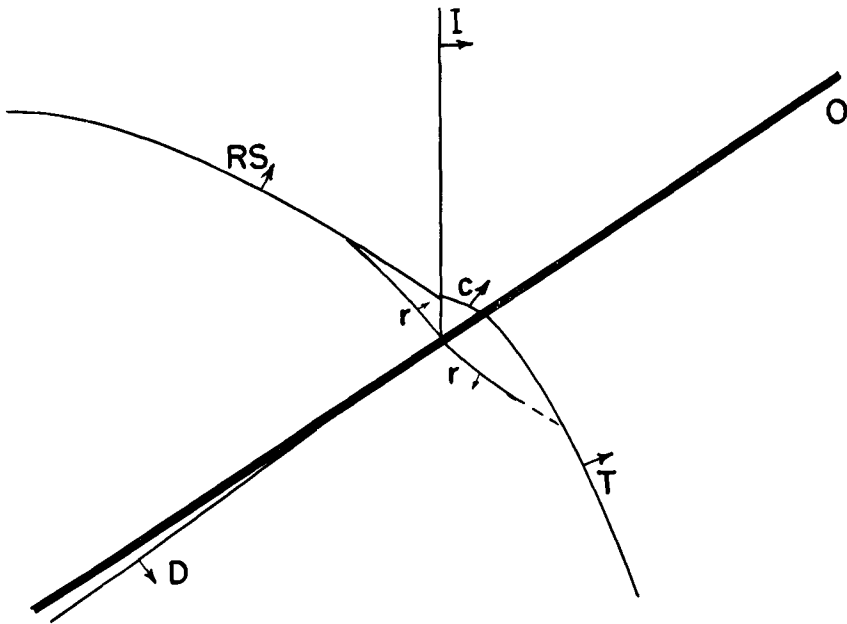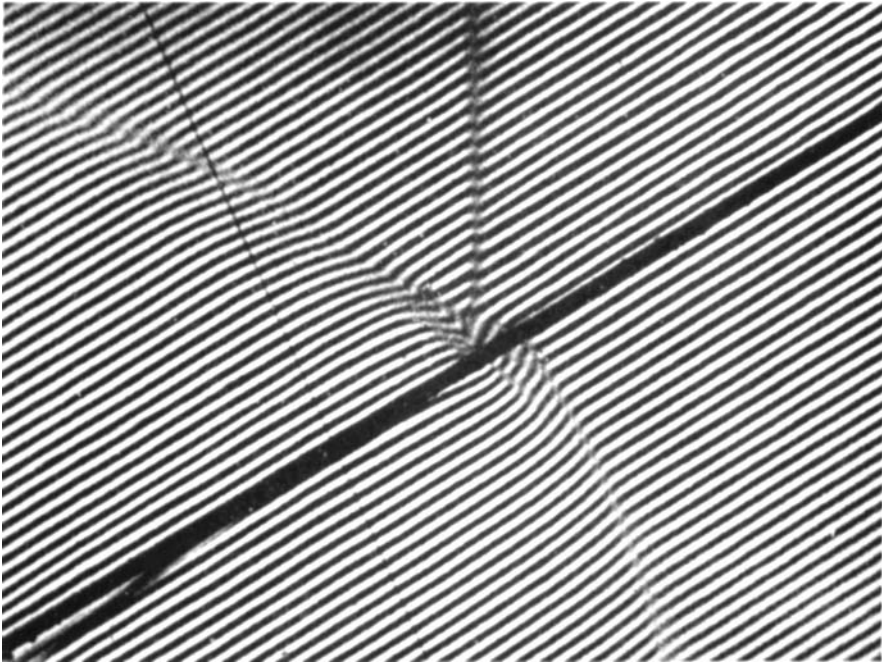
Figure 14 (b). Air/CH_4, irregular refraction, $a > \alpha_c$. (I, RS, T = incident, reflected, transmitted shocks ; O, D = original, deflected interfaces; r = sonic rarefaction front.)
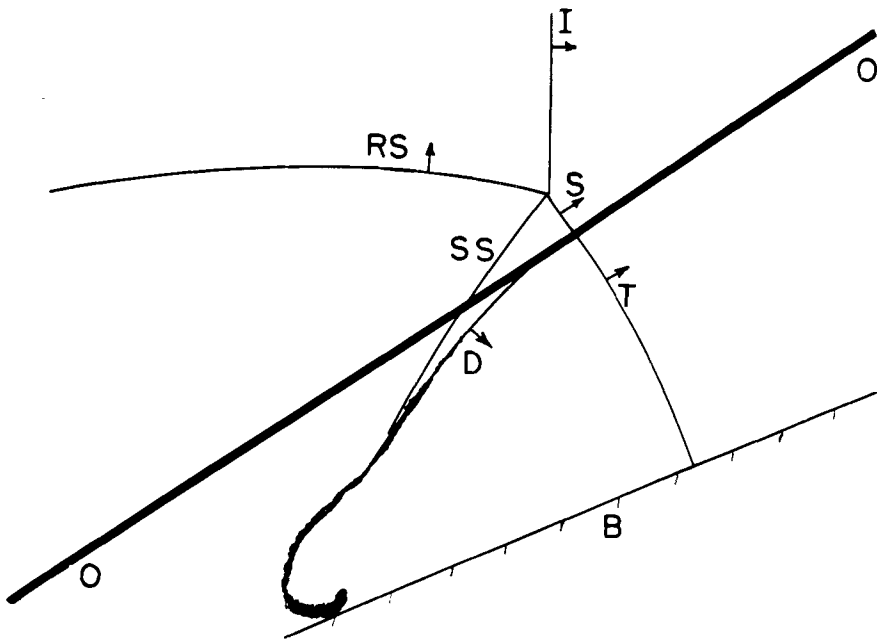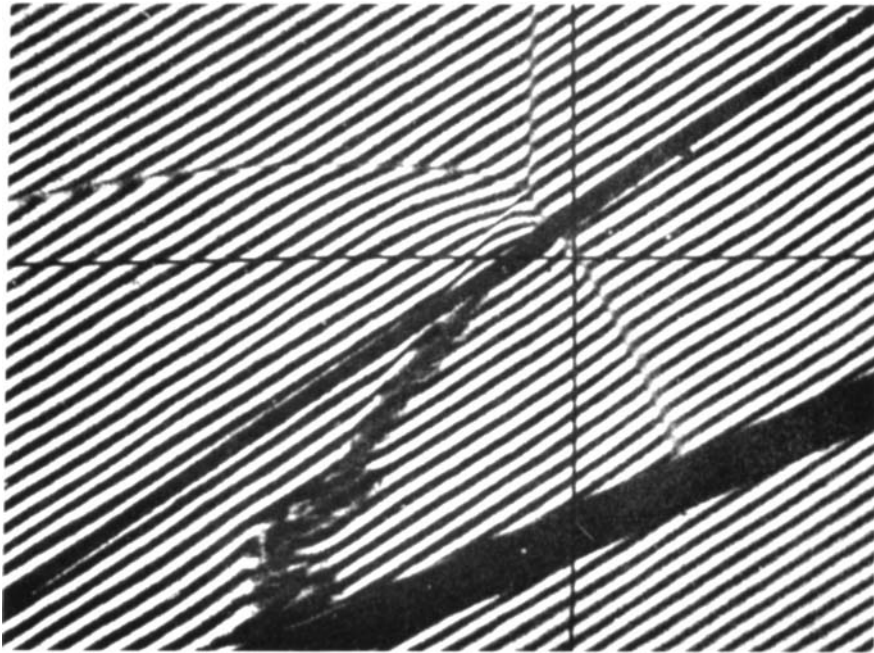
Figure 14 (c). Air/CH_4, irregular refraction, $\alpha > a_A$. (I, RS, T = incident, reflected, transmitted shocks; O, D = original, deflected interfaces; S = stem shock; SS = slipstream; B = back plate.)
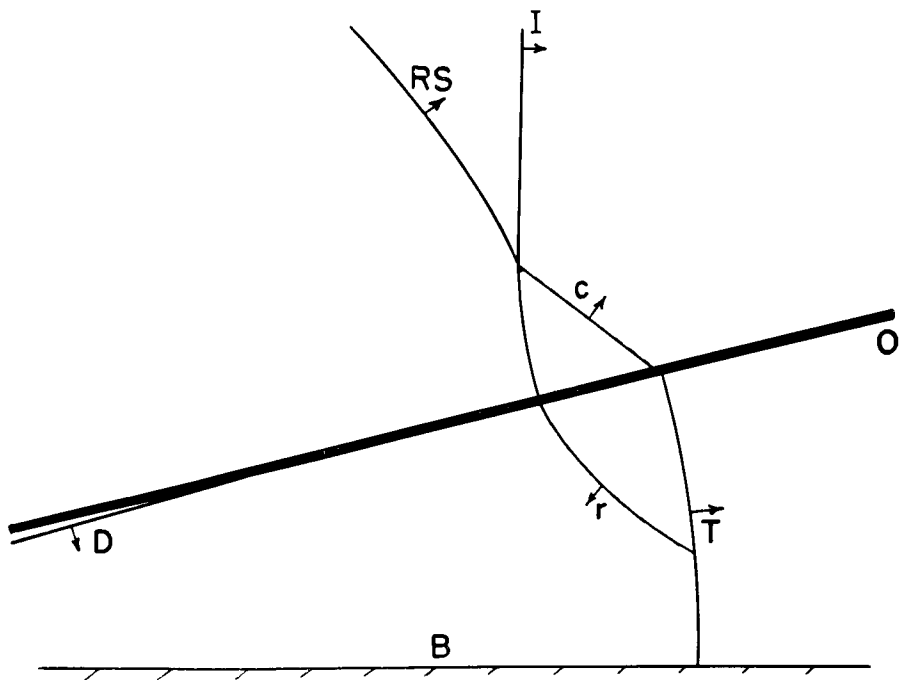
Figure 14 (d). Air/CH$_4$, irregular refraction, $\alpha > \alpha_i$. (I, RS, T = incident, reflected, transmitted shocks; O, D = original, deflected interfaces; c, r = sonic compression, rarefaction fronts.)
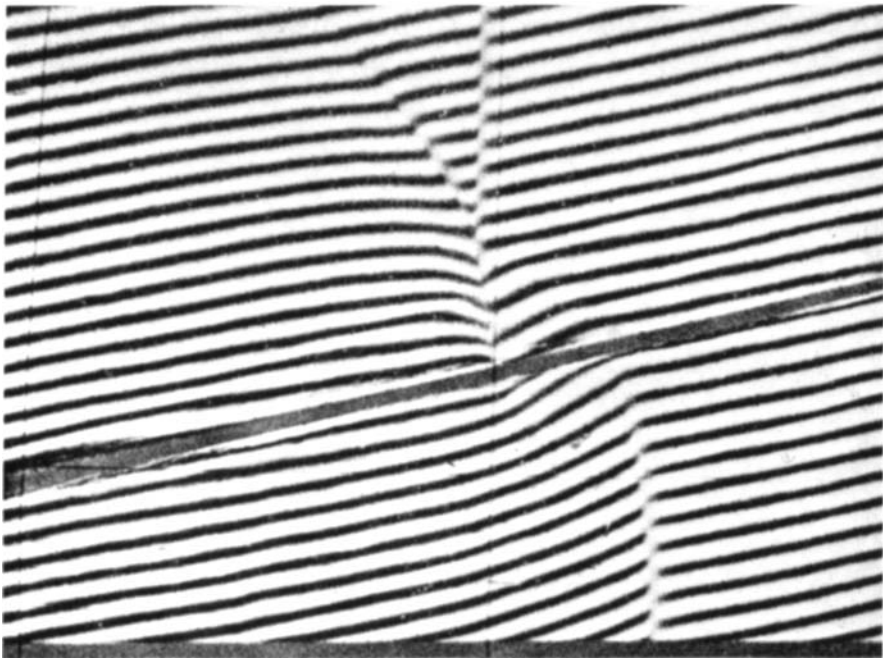
Figure 14 (e). Air/CH$_4$, irregular refraction, $\alpha > \alpha_j$. (I, RS, T = incident, reflected, transmitted shocks; O, D = original, deflected interfaces; B = back plate; c, r = sonic compression, rarefaction fronts.)
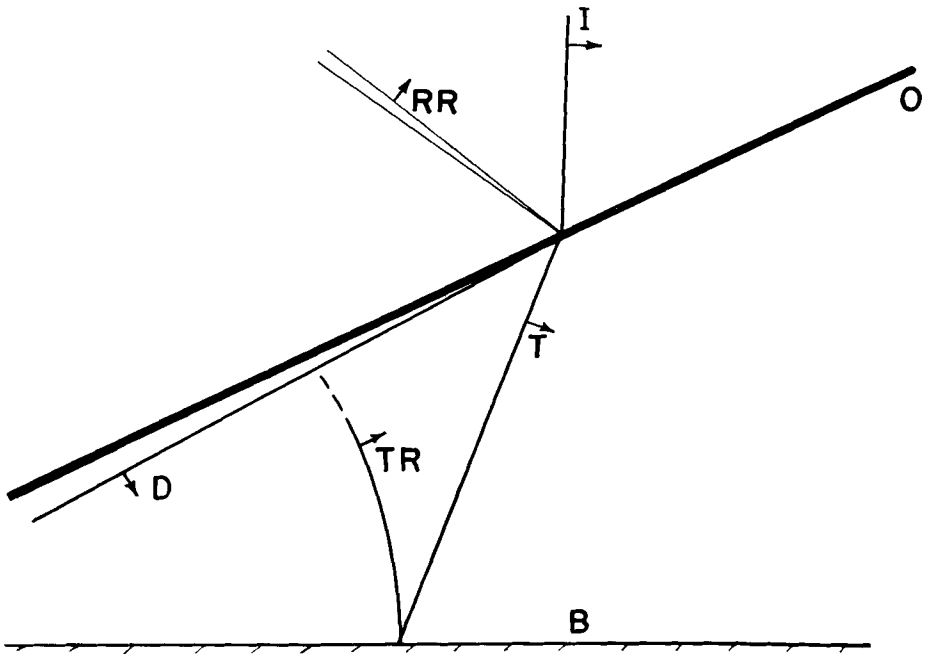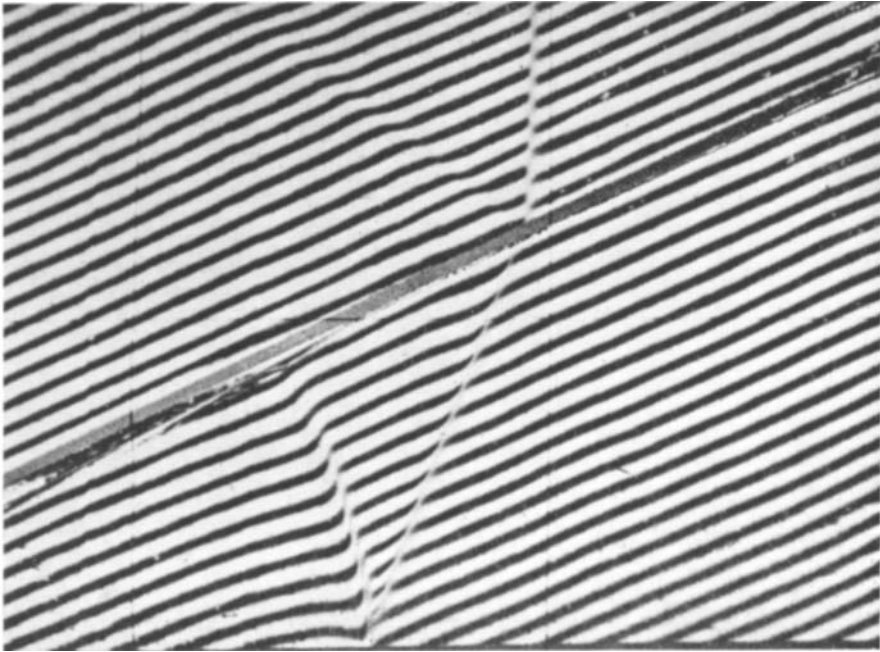
Figure 14 (f). Air/CO_2, regular refraction (I, T = incident, transmitted shocks; RR = reflected rarefaction; O, D = original, deflected interfaces; B = back plate; TR = reflection of T from B.)
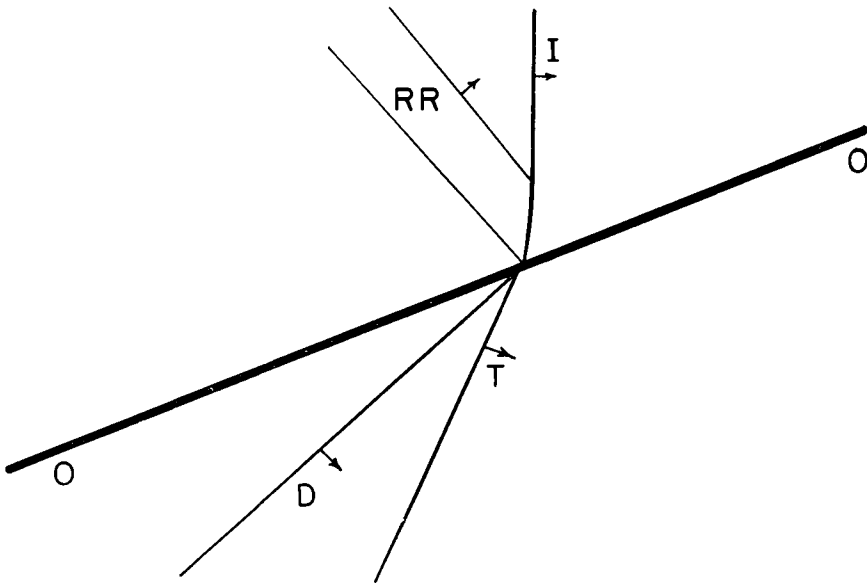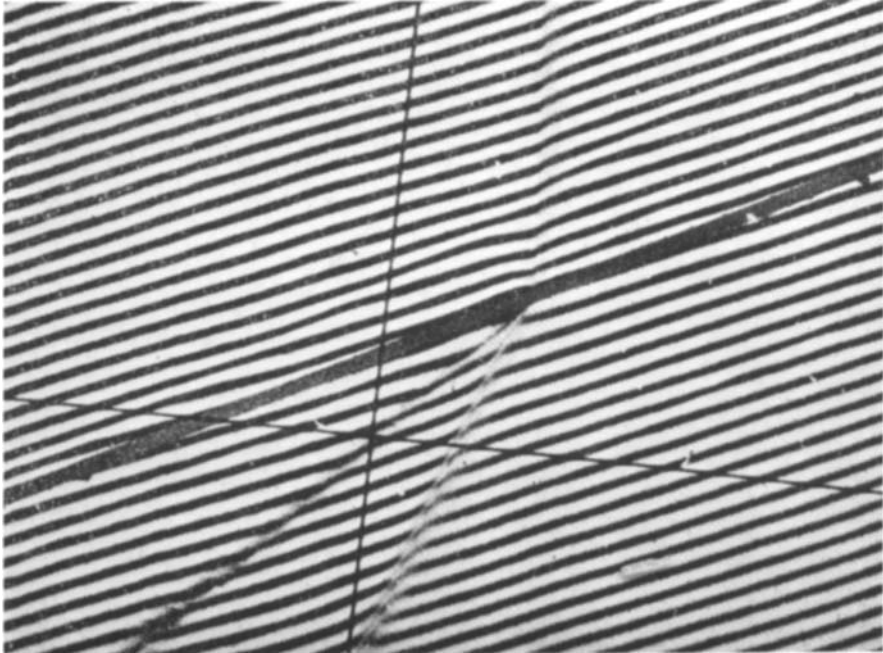
Figure 14 (g). Air/CO_2, irregular refraction, $\alpha > \alpha_a$. (I, T = incident, transmitted shocks; RR = reflected rarefaction; O, D = original, deflected interfaces.)

Robert G. Jahn, The refraction of shock waves at a gaseous interface, Plate II.
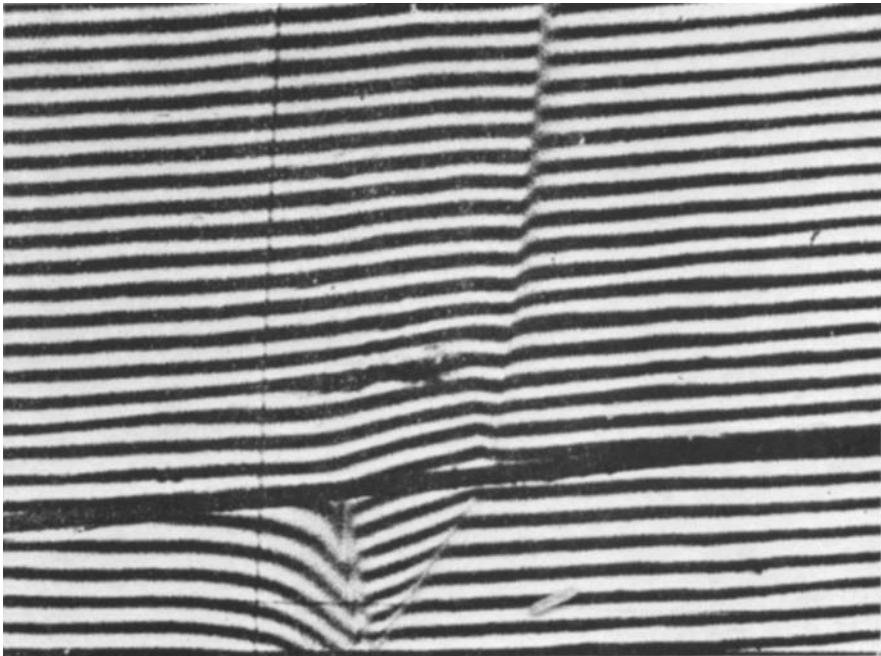
Figure 14 (h). Air/CO$_2$, irregular refraction, $\alpha > \alpha_{//}$. (I, T = incident, transmitted shocks; RR = refle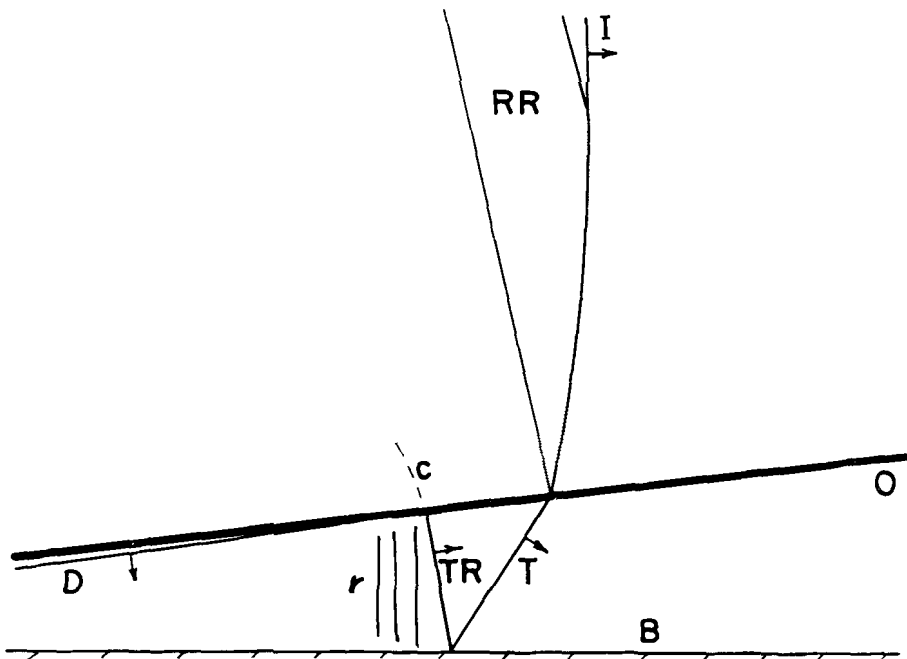cted rarefaction; O, D = original, deflected interfaces; B = back plate; c, r = compression, rarefaction fronts; TR = reflection of T from B.)
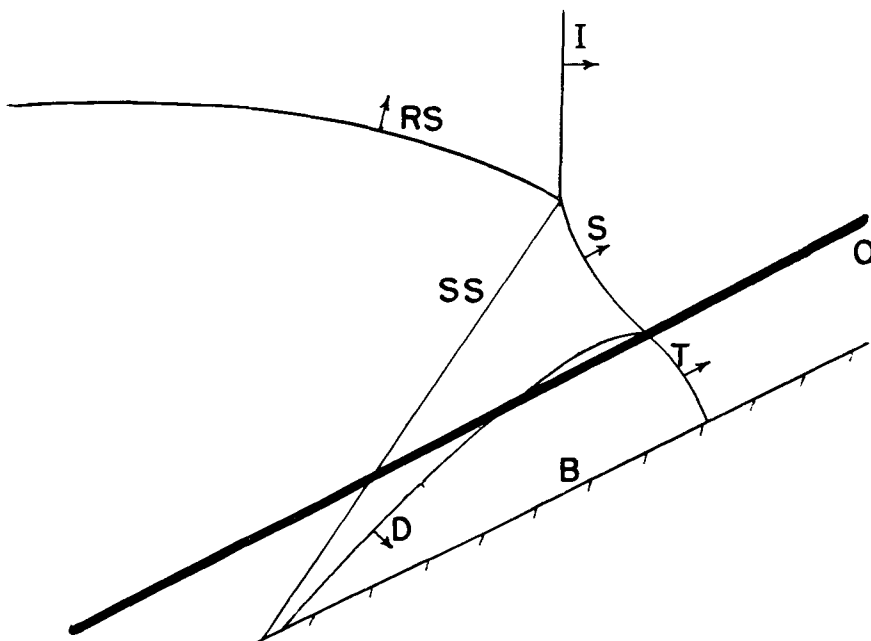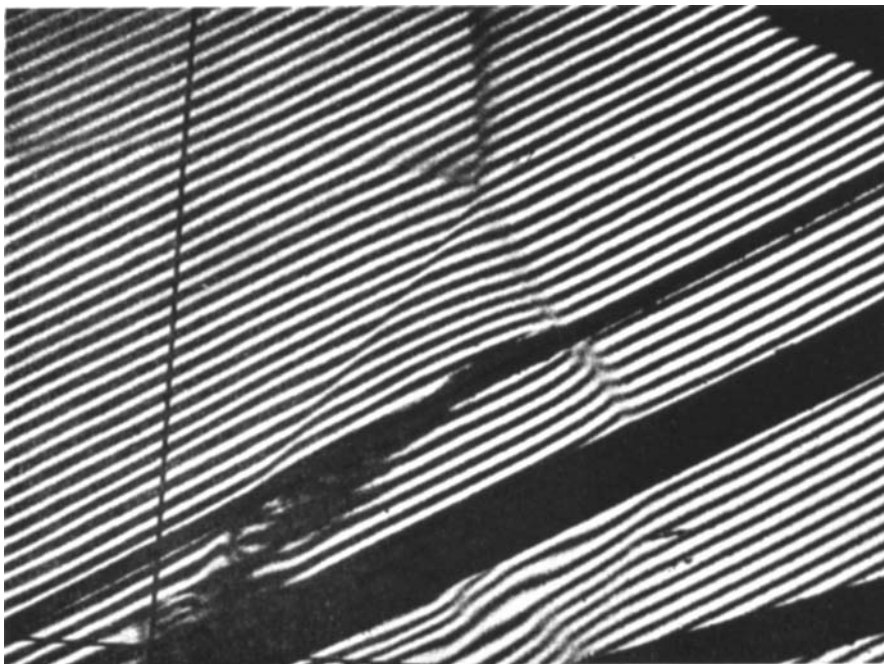
Figure 18. Irregular refraction interferogram for air/CH$_4$ with $\xi = 0.30$, $\alpha > \alpha_i$, and back plate B set parallel to the original interface O—a simulation of a thermal boundary layer.

normal refraction case, specifically to measure γ for either the refracting gas or air. For example, in going to progressively stronger incident shocks, it would be possible to study the dependence of γ on temperature. (These ideas were first suggested to the author by Professor W. Bleakney.)

The agreement between the theoretical and experimental values again permits endorsement of the Polachek & Seeger computations, and their choice of the physically realistic branch of the numerical solutions, for the
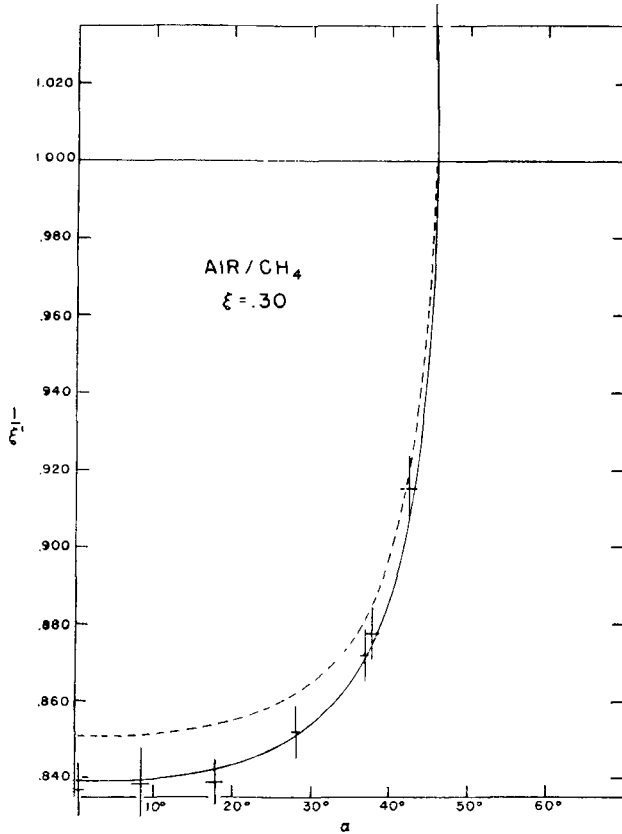
Figure 9. Experimental values of $1/\xi'$ superimposed on theoretical predictions, for air/CH$_4$ with $\xi = 0.30$. For explanation of dotted and solid curves, see figure 5.

specific cases studied here. More generally, by the reasoning offered in § III, it can now be inferred that the theory of regular refraction from which these computations were made is valid for any shock strength from the acoustic limit, $\xi = 1.00$, to $\xi = 0.30$, and for any gas combination having constant values of γ_1, γ_5, and a_1/a_5 in this range of values of ξ.
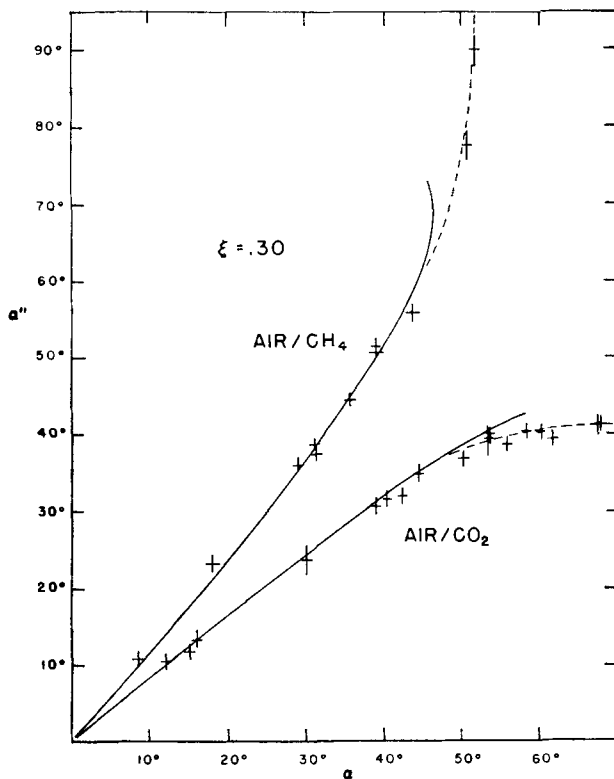
Figure 10. Experimental values of α'' superimposed on theoretical predictions, for air/CO_2 and air/CH_4 with $\xi = 0\cdot30$. Solid curves are adjusted Polachek & Seeger (1951) solutions. Dotted lines follow experimental points into irregular refraction regions.

VI. EXPERIMENT 3 : IRREGULAR REFRACTION

In the mathematical formulation of the theory of shock wave refraction there arise certain upper limits on the angle of incidence α, beyond which no real solutions can be obtained for the assumed configuration. The region from $\alpha = 0$ to the smallest of these limiting angles for a particular refraction problem is defined as the region of regular refraction for that problem. So far our experiments have been concerned exclusively with this region and have indicated the validity of the refraction theory within it. We now consider the refraction problem for angles of incidence beyond the limiting angles, where the idealized theory becomes inadequate.

The failure of the theory to produce realistic solutions beyond the first limiting angle implies physically that the assumed regular refraction process has been replaced by some other type of interaction. Actually, we find experimentally that several different configurations occur in this region, each of them more complex than the regular refractions. These irregular interactions are a significant part of the overall refraction problem. In no

case do the regular refraction solutions persist through to $\alpha = 90°$; in fact, for many reasonable gas combinations, the first limiting angle is quite small, so that the irregular regions for these problems are larger than the regular ones. For this reason alone, some survey of the irregular phase is needed to complete the experimental refraction study. But even beyond their significance in the specific problem, irregular refractions are interesting phenomena in their own right.

In presenting the results of this group of experiments, the approach will be simply to display examples of the various types of configurations that were observed in the irregular refraction regions, and describe the principal features of each pattern. Then, in the absence of any quantitative theory with which to compare the observations, it is interesting to consider, at least qualitatively, the correspondence between the theoretical limiting conditions of regular refraction theory and the irregular patterns that result when those conditions are exceeded. For example, it is possible to show that the various patterns are related to each other in a continuous sequence, and that they may be considered to evolve from one to another, beginning with the regular pattern, under the influence of those aerodynamic require-ments which bring about the limiting conditions. In order to appreciate this relation of the irregular patterns to the limiting conditions, it is best first to discuss the theoretical critical angles and the physical restrictions they represent.

Recalling the formulation of the regular refraction problem outlined in § II, it is possible to anticipate several situations which will make one or more of the assumptions of the idealized model untenable. These may be discussed most conveniently in terms of the smallest angles of incidence at which, for fixed values of the other parameters, the complicating effects first occur. These limiting angles are as follows.

(i) α_a *and* α_A

The theory assumes that the reflected wave will be either a radially straight shock, or a Prandtl–Meyer expansion fan, both centred on the point of intersection of the incident shock with the gas interface. For sufficiently large α, however, region (2) becomes subsonic with respect to the point X. Hence, the angle at which this situation begins is a limit on the assumed configuration. Note that this angle, denoted by α_a, depends only on the value of γ for gas (1) and on the incident shock strength. Actually, if the reflection is a shock, the limit α_a is not strictly appropriate. Rather than require the outflow from the incident shock to be just sonic with respect to the reflection, we should require the flow to be sufficiently super-sonic to permit the existence of the finite shock demanded by the pressure and deflection conditions. For example, for $\xi = 0.30$ in air, $\alpha_a = 61.5°$; however, for air/CH_4, a reflected shock with $1/\xi' = 1.20$ occurs at this angle. Such a shock requires the inflow Mach number to be approximately 1.09, and hence the true limit, which we denote by α_A, is some 4 or 5 degrees lower than α_a.

(ii) α_i *and* α_j

In those cases where $a_1 < a_5$ ('slow/fast'), α'' normally exceeds α, and thus reaches 90° at some $\alpha < 90°$. Expressed more rigorously, it is a consequence of the assumed pattern that $Ma_1/\sin\alpha = M''a_5/\sin\alpha''$, where M'', the Mach number of the transmitted shock, is fixed, independently of this relation, by the pressure and deflection requirements of the problem. Clearly, if the value of M'' computed from these requirements exceeds $Ma_1/a_5 \sin\alpha$, the value of α'' predicted for the assumed pattern becomes imaginary. Physically this must correspond to a limit on the regular refraction configuration. The angle of incidence at which this effect begins is denoted by α_i, and is given by

$$\sin^2\alpha_i = \left(\frac{Ma_1}{M''a_5}\right)^2 = \left(\frac{a_1}{a_5}\right)^2\left(\frac{\gamma_5}{\gamma_1}\right)\frac{[(\gamma_1+1)+(\gamma_1-1)\xi]}{[(\gamma_5+1)(1/\xi')+(\gamma_5-1)\xi]}.$$

(In calculating this angle for tabulation, Polachek & Seeger (1951) have introduced the approximation $1/\xi' = 1$. In some cases, particularly as $\xi \to 0$, this leads to sizeable error, and even to a misplacing of this limit with respect to the others.)

In one sense α_i corresponds to the angle of total internal reflection in optics, since, at this angle, the transmitted signal is travelling parallel to the interface. The analogy is incomplete, however, since in no case short of an infinite impedance ratio across the interface will the incident shock be totally reflected.

It is expedient to define another critical angle α_j which is related to, but always larger than, α_i by

$$\sin\alpha_j = \frac{Ma_1}{a_5}.$$

When $\alpha = \alpha_j$, the point of intersection of the incident shock, X, travels along the interface with a velocity just equal to a_5. For $\alpha > \alpha_j$, therefore, region (5) becomes subsonic with respect to this intersection point, and consequently the transmitted wave can no longer be a shock. Also, some of the region *ahead* of X, both in (5) and (1), can now be influenced by things happening at and behind X.

(iii) α_e

There exists one other limit, which is somewhat more intrinsic than the others, in that it concerns the extent of compatibility of the pressure and deflection requirements. Stated simply, as α becomes larger, an angle of incidence is reached beyond which it is no longer possible to satisfy both the pressure and deflection requirements by any arrangement of strengths and positions of the reflected and transmitted waves. The situation is sufficiently analogous to the extreme angle occurring in the theory of regular reflection to justify the same notation, α_e, for this regular refraction limit. Beyond this angle, the equations produce no real solutions. In most cases, the theoretical curves of $1/\xi'$ *vs* α double back to presumably unrealistic alternative values of ξ' at α_e.

The significance of α_e is increased by the fact that it invariably precedes α_i for any gaseous refraction. The proof of this can be stated very simply. At $\alpha = \alpha_i$, $\alpha'' = 90°$, hence δ'', the deflection of the flow by the lower path, is zero. Then, in order to have $\delta + \delta' = \delta''$, δ' must be equal to $-\delta$, and this is obviously impossible with ξ' an order of magnitude weaker than ξ. Therefore the α_e-condition must have occurred before $\alpha = \alpha_i$. In other words, a regular refraction pattern with $\alpha'' = 90°$ cannot be achieved.

Thus it must be α_e or α_a (or α_A, whichever is appropriate) that establishes the extent of the regular refraction regime and introduces the first irregular pattern. The order in which these limits occur depends on both the gas combination and the incident shock strength. For most combinations in which a_5 is substantially larger than a_1, the deflection condition becomes critical before region (2) becomes subsonic. In these cases, α_e occurs first. For most combinations in which $a_5 \doteq a_1$, or $a_5 < a_1$, however, the limiting angles α_e and α_a (or α_A) are quite close and the order of their occurrence depends on the incident shock strength†.

(At this point it might be argued that, for any given refraction problem, all limiting angles except the first have only academic significance, for they are derived as limits to a regular refraction process which terminates before they are reached. While it is true that the numerical values of these angles computed on this basis are not entirely realistic, the requirements on the refraction process that they represent are still pertinent, even for the irregular configurations, and the effects resulting from violating these requirements are observed experimentally at sufficiently large α. In fact, the effects associated with exceeding α_i and α_j, which can never be the first limiting angles, are the most pronounced of all the irregular interactions.)

(*iv*) α_{sr} *and* α_{st}

In any physically realistic refraction situation, it is also necessary to consider two other practical limits to the existence of a regular pattern. As mentioned in §III, the ideal regular configuration can be realized experimentally only so long as the outflow in regions (3) and (4) is fast enough to prevent signals from the 'corner' from overtaking the intersection point. Beyond some limiting angle of incidence, this condition cannot be met and various signals, associated with the physical corner at which the refraction process began, are able to overtake and contaminate the region of interest in the pattern. This complication is not, of course, peculiar to the refraction problem. Almost any two- or three-dimensional shock interaction experiment must reckon with this situation in one form or another (in particular the Mach reflection problem, cf. Fletcher, Taub & Bleakney 1951). The persistent occurrence of corner interference in such problems has often inspired philosophical discussion about the futility of considering them without complete specification of the physical corners at which the processes will begin. Rather than digress into that arena, however, we will merely state here the nature of the corner signals in the refraction problem, and indicate methods of treating this complication†.

In a refraction problem, the corner signal may be either a compression
or a rarefaction front. Its phase and strength are determined by (i) the
phase and strength of the reflected wave, (ii) the interaction of the transmitted
shock with the back boundary, and (iii) the nature of the mechanical corner
formed by the leading plate and back plate, around which the flow behind
the transmitted shock must deflect (see figure 11). In a sense, each of
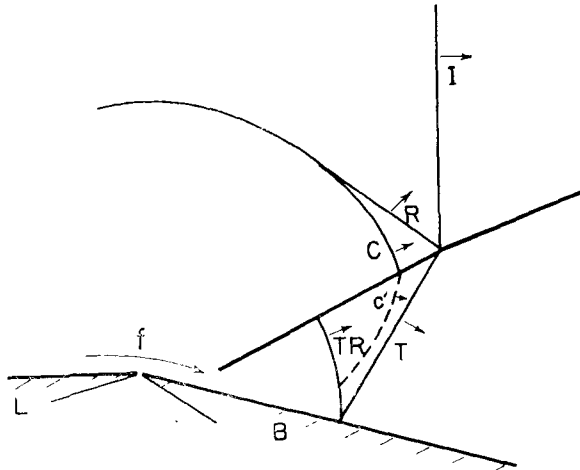

Figure 11. The corner signals in a refraction experiment. The reflection TR of the
transmitted shock T, the deflection of the flow f around the corner formed by
the leading plate L and the back plate B, and the finite length of the reflected
wave R, each contribute to a composite corner signal C which radiates from
the corner with the local speed of sound in the two gases. In general, these
speeds differ, and hence a secondary signal c' is transmitted across the deflected
interface from the faster to the slower medium, ahead of the original corner
signal in that medium.

these three effects contributes a component to a composite corner signal
which radiates from the point of origin of the process with the local velocity
of sound, compounded vectorially with the flow velocity.

It is the 'catching up' of this composite signal with the intersection
point in the incident and refracting media that constitutes the experimental
limits α_{sr} and α_{st}. If this corner signal is a net rarefaction, the effect of its
overtaking a shock will be to weaken the shock and curve it backward (making
it less normal to the flow); if it is a net compression, it will tend to strengthen
the shock, thereby curving it forward (more normal to the flow).

Note that the strength and phase of the first component is fixed auto-
matically for a given refraction situation, but that the latter two are under
the control of the experimenter who, by changing the angle of the back
plate, can vary the strength of these components and hence the strength of
the composite signal. In practice, use was made of this valuable feature *via*
two complementary procedures which served to separate the effects associated
entirely with the idealized irregular refraction process from those which are
dependent on the corner situation.

(i) A given irregular refraction was performed with the back plate set to form a corner signal which was a net compression. The same refraction was performed with the back plate reset to form a net rarefaction corner signal. Those effects which appeared the same for both cases were assumed to result solely from the refraction process.

(ii) The back plate was adjusted so that the various contributions to the corner signal compounded to zero in the region of interest. This could be done by setting the back plate to some intermediate angle such that the net contribution from the mechanical corner and the transmitted wave interactions just balanced the uncontrollable component associated with the reflection process. In this way, the most interesting part of the refraction pattern could be observed, free from corner interference.
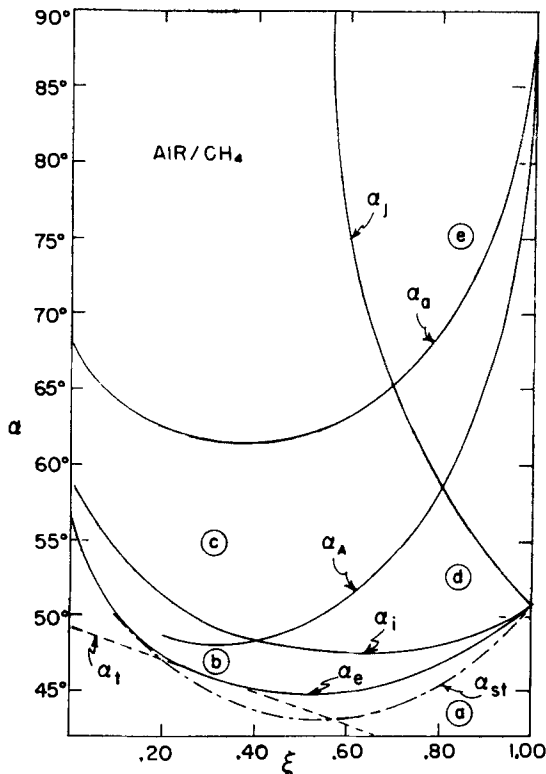

Figure 12. The critical angles for air/CH$_4$ vs incident shock strength. Circled letters refer to corresponding interferograms in figure 14 (plates 4 to 8).

The considerations outlined above suggest the following physical behaviour. As the angle at which the shock impinges on a specific gas/gas interface is made more and more glancing, an angle of incidence is reached— the first limiting angle for the case involved—beyond which the regular refraction pattern cannot occur, but is replaced by a new configuration. We expect that this new configuration will be related to the regular pattern it has replaced, in fact that it will be a distortion of it, and that this distortion

will be such that the flow requirements that brought about the demise of the regular pattern are now reconciled. As the angle of incidence is increased further, a limiting condition for this irregular pattern may be reached, at which point a new distortion of the configuration must occur to accommodate the second critical requirement. The pattern will continue to evolve in this way, adjusting itself to each new requirement by some distortion, until α reaches $90°$.

In figure 14 (plates 4 to 11) are displayed samples of the super-critical patterns that were observed for the air/CO_2 and air/CH_4 gas combinations. Figures 14a to 14e show an essentially complete series of irregular configurations for air/CH_4, arranged in order of increasing angle of incidence. Figures 14f to 14h show a similar series for air/CO_2. Each interferogram is accompanied by a line diagram to clarify the position and nature of the various signals involved in the interaction.
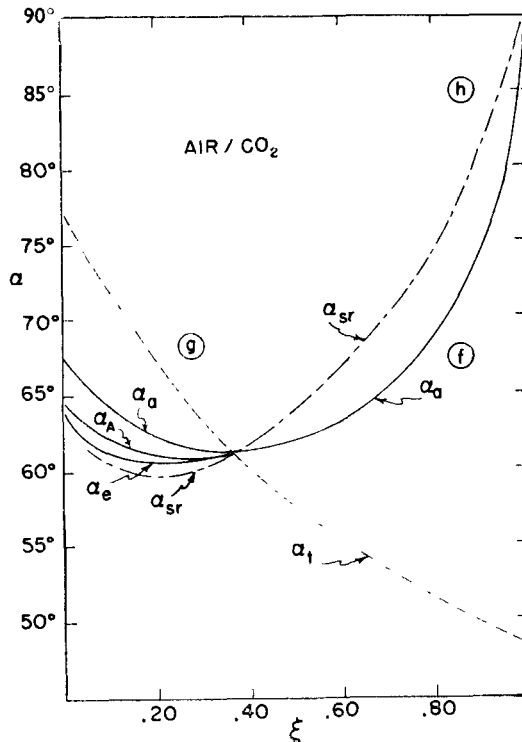
Figure 13. The critical angles for air/CO_2 *vs* incident shock strength. Circled letters refer to corresponding interferograms in figure 14 (plates 9 to 11).

The relation between a given configuration and the various critical angles may be visualized by reference to figures 12 and 13, in which are plotted the pertinent critical angles as functions of the shock strength for the two sets of gases. On these figures, the regions characterized by the subsequent interferograms are indicated by circled letters corresponding to

the appropriate patterns in figure 14. Note especially that the critical angles have substantially different values at the two shock strengths used, namely $\xi = 0.85$ and $\xi = 0.30$. This feature, and the previously mentioned extra degree of freedom available in the back boundary, were utilized extensively to separate the various irregular refraction effects from one another and from the corner effects†. In a few cases, two critical angles fall so closely together that it is not possible to separate out their two effects by a single picture taken between them, and less direct methods have had to be used to study that region. Nevertheless, it has been possible to construct, from interferograms such as these, a rather complete catalogue of the irregular refraction effects and their relation to specific critical conditions. This may best be illustrated by brief separate discussions of each of the patterns.

The air/CH_4 irregular refraction patterns

Figure 14a (plate 4) shows the regular refraction pattern that exists for the air/CH_4 combination just below the first critical angle. Note that all three shocks are straight, and that the angular regions between them are uniform in the neighbourhood of the intersection point. In the regions behind the reflected and transmitted waves, it is possible to observe a weak rarefaction front. This is the corner signal for this particular arrangement of the boundaries; at this angle of incidence it has not been able to overtake the region of interest.

As the angle of incidence is increased, the first limiting angle to be exceeded is α_e. Figure 14b (plate 5) shows the pattern that is observed for this situation at $\xi = 0.30$. Since α_{st} has also been exceeded, it becomes necessary to investigate the extent to which the corner signal is contaminating the refraction pattern. In practice this was done by comparing many patterns taken in this same irregular region, at different shock strengths and with different settings of the back boundary, to separate out those effects which were boundary-dependent and hence not directly related to the exceeding of the α_e-condition†. This done, the following features of figure 14b remain attributable to the refraction process.

The reflected wave RS is curved all the way into the intersection, and its strength increases very rapidly near the intersection. In its region of greatest strength, RS is followed by a sharp expansion region, which has the effect of 'peaking' the reflected shock, the front of which is now comparable in strength to the incident shock! Curiously enough, none of the other regions or signals in the pattern are appreciably disturbed. Even the deflected interface, which is adjacent to the outflow from this anomalous reflection, is still radially straight from the intersection point.

It is best next to consider the effect of exceeding α_A, which is shown in figure 14c (plate 6) for $\xi = 0.30$. When adequate compensation for the corner effects has been made, in a similar manner to that described above, the following features of the pattern remain pertinent to the refraction process for this case.

A configuration much like a Mach reflection exists on the air side of the interface, complete with a Mach stem, a curved, varying strength reflection, and a slipstream from the triple point. The reflected signal and the stem are both peaked near the triple point. The deflected interface is now curved along its entire length and approaches quite close to the slipstream as the two near the back plate. Thereafter they both exhibit an almost turbulent curling.

The effect of exceeding α_i is not very noticeable at the stronger shock strengths, and α_j is imaginary there, so to study these we returned to the case $\xi = 0\cdot 85$. The onset of the process is shown in figure 14 d (plate 7). Note that several significant alterations have taken place. The transmitted shock has degenerated, near the interface, into a continuous compression, the leading edge of which is overrunning the intersection point of the incident shock slightly. A compression pulse has been retransmitted into region (1), ahead of the incident shock I. This, in turn, deforms I near the interface. The reflected shock and the sharp rarefaction region following it (cf. 14 c, plate 6) have been distorted into a complex pulse, the leading edge of which has advanced up the back of I to the point where I intersects the retransmitted compression.

As the angle of incidence increases still further, the effects just described become more distinct. For example, figure 14 e (plate 8) displays the situation for $\alpha > \alpha_j$. In this case, the inflow in region (5) on the transmitted wave would not be even sonic if T did not run out ahead. Two differences may be noted between this pattern and that for $\alpha > \alpha_i$. The transmitted shock has now degenerated completely into a compression front at the interface. Also, the reflection is a cleaner shock, and the rarefaction following it is much less steep, than those appearing in the previous case.

The air/CO_2 irregular patterns

The irregular refraction region for the air/CO_2 problem is considerably less complex. The only pertinent limiting angles are α_e and α_a (and α_A for $\xi < 0\cdot 37$), and, as may be seen in figure 13, the curves for these, along with that for α_{sr}, are crowded together in a narrow band over most of the range of values of ξ. Nowhere is the angular interval between α_e and α_a (or α_A) large enough to permit an observable development of the irregular effect related solely to the former, before it is obscured by the rather prominent effect arising from the latter. Consequently, it is possible to observe only one type of irregular pattern for this problem—one that exhibits primarily the effect of exceeding the α_a-condition. This is a rather interesting case, however, since it displays the transition of the reflected rarefaction from a supersonic to subsonic phenomenon.

An example of the regular refraction pattern that exists at values of α just below α_a is shown in figure 14 f (plate 9). The irregular pattern that appears when α_a is exceeded follows in figure 14 g (plate 10). The principal changes to be noted concern the reflected rarefaction which, by the definition of α_a, now finds itself in a subsonic region. RR is no longer a centred wave,

but its leading edge has advanced into region (2), having climbed a short distance up the back of the incident shock I. (This intersection of the leading edge of RR on I subtends an angle at the corner which is approximately equal to α_a.) That portion of I that is overtaken by this rarefaction edge is weakened by it, and consequently curved backward slightly, causing it to make a smaller angle with the interface. The back edge of the rarefaction remains fixed at the intersection point. With these exceptions, the remainder of the fields (2) and (3) are uniform, as in regular refraction.

As α is increased further into the irregular range, the situation described above changes in magnitude only, with no other noticeable effects appearing.

The pattern shown in figure 14g was obtained with the back plate set normal to the transmitted shock. To illustrate how the corner effect from a less favourable boundary arrangement can confuse the refraction process, consider figure 14h (plate 11), which was obtained with the back plate set normal to the incident shock. In addition to the effects observed in the preceding pattern, there now appears a compression region behind the reflection—a feature which was totally absent in the other cases. Apparently this results from the draining of the excess pressure behind TR across the interface into the upper region (3), in which the compression can travel fast enough to reach the reflected wave. Some of this effect even extends back across the interface into the region (4) behind T, making it also non-uniform. The relief of the pressure behind TR is evidenced by the strong rarefaction following it. From another point of view, the shock TR can be considered to be refracting, irregularly, at the CO_2/air interface, producing a configuration not unlike that seen for air/CH_4 at glancing incidence (cf. figure 14e, plate 8).

The interpretation of the irregular patterns

From the experiments we know that each irregular refraction pattern is a pseudo-stationary equilibrium configuration; that is, the pattern grows linearly with time†. As such, the process can be treated as a steady state when expressed in distance/time coordinates. A formal theory of this interaction would have to derive the steady-state configuration from basic principles and initial conditions, just as was done for regular refraction. In this case, though, the assumed models would need to be quite complex, and the resulting computations correspondingly complicated. However, since we are dealing with a pseudo-stationary problem, some qualitative predictions can be made from perturbation considerations. From the experiments we have seen that the various configurations that develop as the angle of incidence is increased are related to one another in a continuous fashion, forming, as it were, a sequence, or evolution of patterns, rather than exhibiting any abrupt changes in detail. Hence, it should be possible to infer the nature of any one of them from a knowledge of an adjacent pattern, and consideration of the flow conditions that necessitate the change.

As an illustration, consider first the one observable irregular pattern for air/CO_2. The regular pattern observed for α just below α_a is shown in

figure 14 f (plate 9). Now, perturb this stable configuration slightly by increasing α until it is larger than α_a and then readjust the pattern accordingly until a new equilibrium condition is achieved, as follows.

When α exceeds α_a, the gas flow in region (2) becomes subsonic relative to the reflected rarefaction RR. Therefore, the Prandtl–Meyer wave, which requires sonic flow normal to all its radial characteristics, can no longer exist as such. Instead, the leading edge of the rarefaction is free to run ahead into region (2). Consequently, this front, remaining straight but no longer centred at the intersection point X, will overrun part of the incident shock I. If α is not too much greater than α_a, the expansion will still be sufficient to return the flow to sonic velocity behind RR, and the trailing edge will retain its centred position.

That portion of I near the interface that has been overrun by the rarefaction will now be weaker and hence more inclined to the incoming flow there. The effect, thus, is to curve I from the interface up to the intersection with the rarefaction front, causing it to be incident at a smaller angle on the interface. The pattern just constructed is essentially that observed experimentally (figure 14 g, plate 10).

A similar line of reasoning can be applied to the series of air/CH_4 irregular refraction patterns. The first critical condition is associated with the α_e-limit, the violation of which results in the most subtle, yet probably the most significant, of all the irregular effects. If we make α slightly larger than α_e, we impose upon the reflected shock RS and the transmitted shock T incompatible pressure and deflection conditions. The essence of the situation is that, if we required RS and T to meet the pressure requirements ($p_3 = p_4$), the outflows in regions (3) and (4) would be convergent.

A clue to the resolution of this paradox can be taken from a distantly related situation. In the problem of the supersonic aerofoil, for a given flight velocity, there is a limiting body angle beyond which a straight bow shock cannot deflect the flow parallel to the surfaces. For cases above this limit, the observed behaviour is that the bow shock becomes stronger near the leading edge, and less inclined to the flow there. This stronger shock produces a subsonic rather than supersonic region behind it, in which subsonic region the necessary flow deflection is taken care of continuously. (Strictly speaking, it cannot be continuous right in the corner between the shock and the boundary. Here the 'continuous' variation must be condensed into an infinitesimal region—a common type of subsonic singularity, cf. subsonic flow over a sharp corner.) This subsonic region is clearly an expansion, and is most severe where the shock is strongest. If the body angle is increased yet further, the bow wave detaches from the leading edge, and advances into the oncoming flow.

The reflected shock in the supercritical refraction pattern apparently cures its deflection difficulty by essentially the same process, that is, it becomes stronger and less inclined to the inflow, and in so doing produces a subsonic region behind it which handles the deflection and presssure adjustment in a continuous fashion (see figure 15).

This mechanism can only exist as shown over a small range of α. As α is increased further, the gas flow in region (2) relative to the reflection becomes less supersonic, and this reflected strong shock must become more normal to it to maintain its strength. Beyond the situation where it is just normal to the inflow, it has no other course than to leave the intersection point and advance into region (2), much as the bow wave detaches from the aerofoil. This, of course, is just the α_A-limit, beyond which a new irregular pattern occurs.
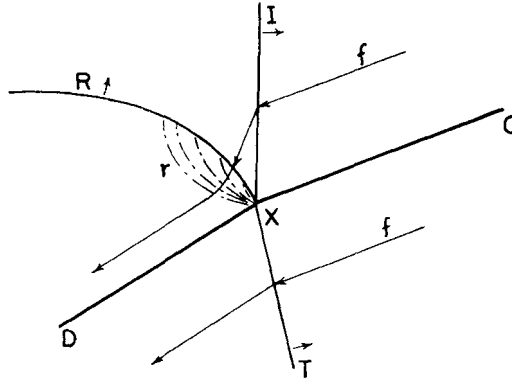

Figure 15. The α_e-adjustment. The reflected shock R becomes stronger near the interface, and is followed immediately by a steep subsonic rarefaction zone, which completes the necessary flow deflection and pressure adjustment.

That the process described above is far from insignificant is clear from the observed patterns of figure 14 b (plate 5) which show the great increase in strength of RS near the interface, and the sharp rarefaction region behind it. It is also impressive to compare the measured magnitude of this shock front near the interface with the reflected wave strengths in regular refractions (see figure 16).

It would seem only reasonable that some process like that developed above would likewise be expected in connection with the transmitted shock—to help out, as it were, with the flow deflection problem. Yet it remains a curious point in this case that there is no observable participation of the transmitted shock, and the flow behind it, in this readjustment process. As far as can be seen from the interferograms, T remains straight and unchanged in strength, and the field behind it remains very nearly uniform even though a rather drastic process is taking place in the adjacent region. Even the deflected interface seems totally unperturbed.

The α_A-adjustment for the air/CH_4 problem follows directly from the α_e-configuration just discussed. When α exceeds α_A, the gas flow in region (2) is no longer fast enough with respect to RS, even when normal to it, to maintain it at the required strength. As in the corresponding case for air/CO_2, RS will then advance into region (2) at a speed sufficient to maintain the necessary gas inflow on itself. In so doing, RS overtakes a portion of I,

thereby strengthening it, and establishing a pattern quite similar to a Mach reflection (cf. figure 14 c, plate 6). The difference in entropy change for the gas crossing I and then RS, and that crossing the stem, necessitates a slipstream from the triple point. This slipstream is observed experimentally and is valuable in the interpretation of the patterns, since it assumes the direction of the local flow velocity.
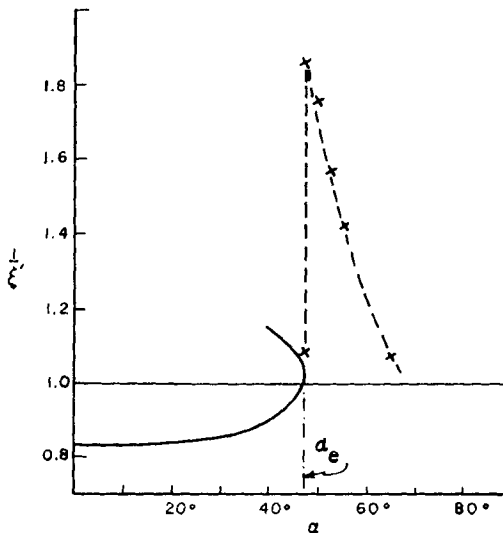

Figure 16. Strength of reflected wave front $(1/\xi')$ *vs* angles of incidence (α) for air/CH₄ with $\xi = 0.30$. Solid line follows regular refraction solutions. Crosses mark experimentally observed strengths. Note the extreme maximum immediately following α_e.

The postulated pattern is quite efficient in relieving the critical conditions that necessitated the alterations. The stem shock is normal to the interface and strong enough to leave a subsonic region behind it, the combination of which handles the deflection of the flow near the interface quite adequately. The reflected wave is now somewhat removed from the interface, and no longer need deflect the flow behind it to be exactly parallel to the outflow from T, since there is a subsonic transition between regions (3) and (4). That this is indeed the case may be seen in figure 14 c (plate 6) where the slipstream from the triple point, which follows the local flow direction, is clearly not parallel to the deflected interface. The less strenuous deflection requirements on RS are reflected in a lessening of its strength, quite sharply, as α increases (cf. figure 16).

For $\xi = 0.30$, the limit α_A is closely followed by α_i, which then is the last pertinent critical angle. However, for the weak shocks ($\xi = 0.85$), α_i precedes α_A by 13° and therefore produces a much more clearly defined effect. For this reason we will construct the α_i pattern at $\xi = 0.85$, with the understanding that a similar situation must occur for the stronger shocks

also. At $\xi = 0.85$, the previous pattern was that developed for $\alpha > \alpha_r$ (cf. figure 14 b, plate 5). As α is increased past α_i, the transmitted shock (which by definition of α_i now makes an angle of $\alpha'' = 90°$ with the interface) finds itself in a region where the inflow velocity is too small for its shock strength. To remedy this, the shock runs ahead in region (5), no longer maintaining contact with the intersection point (cf. figure 17 a). In so doing, however, a pressure difference is set up across the interface between the intersections of I and T. This of course requires a compression signal to be sent upward into (1) ahead of I, and, simultaneously, a rarefaction downward behind T (figure 17 b). The effect of the compressed region ahead of I is to curve I forward, causing it to make a larger angle of incidence with the interface (figure 17 c). The region behind this curved portion of I
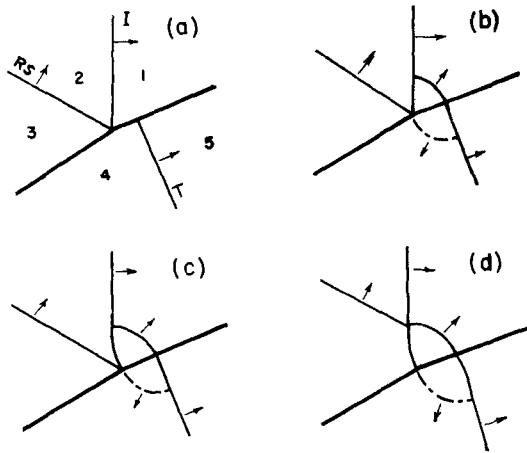

Figure 17. The α_i-adjustments. (a) The transmitted shock T leaves the intersection point and runs ahead into region (5). (b) This causes a compression front to propagate into region (1), ahead of the incident shock I, and simultaneously, a rarefaction front to advance down into region (4) behind T. (c) Consequently, T is weakened near the interface, while I travels more rapidly into the gas passed over by the compression. (d) The region behind the curved portion of I is now subsonic, hence the reflected shock RS runs ahead into region (2), until it reaches supersonic flow again, that is, behind the straight portion of I.

is no longer uniform. In particular, it is no longer supersonic with respect to the reflection, since the angle of incidence of this stem is past the α_A-limit. The process adopted in a case like this, as we have already seen in other cases, is for the reflection to advance into (2), climbing the back of I to the point where an adequate flow normal to itself is available, which in this case should be near the start of the curvature of I (figure 17 d).

The rarefaction that advances into (4) will weaken T somewhat, thereby reducing the inflow requirements slightly. This feature tends to stabilize the situation, in a sense restraining T from getting too far ahead. The

equilibrium situation finds T—a finite shock, followed by a region of compression to p_4—running just slightly ahead of the intersection point of I. The pattern that actually occurs for $\alpha > \alpha_i$ (figure 14 d, plate 7) corresponds to this equilibrium configuration.

If α is increased further, the inflow velocity in region (5) becomes subsonic ($\alpha > \alpha_j$), in which case there is nothing to prevent T from degenerating completely into a continuous compression, the front of which will run ahead with velocity a_5. The resulting other adjustments will be qualitatively the same as those described above for the α_i case, although the interaction region will now be much larger. This is the configuration displayed in figure 14 e (plate 8).

The process cannot proceed to this extreme in the stronger shock case, since the velocity of the configuration along the interface is more rapid, and hence the inflow deficit on T is relatively less significant†.

Figure 18 (plate 12) shows the α_i effect for $\xi = 0.30$. Note that even at this large α (65°), T is only slightly ahead of the incident stem. One of the most interesting features of this picture is that the stem has been deformed by the precursor compression in such a way that it is actually incident at $\alpha > 90°$! As a consequence of this, the flow behind it temporarily has an upward component, and the interface is seen to be deflected up above its original position for a short distance.

It is clear from even such a sketchy analysis as that outlined above that the irregular patterns have a significance beyond their specific application to the refraction problem. In addition to providing some basis for empirical treatment of the irregular refraction regime, they are an abundant source of information on various shock interactions and flow field configurations which, in many cases, would be difficult to observe by more *ad hoc* experiments. In a sense, each irregular refraction process acts as a matrix in which are embedded, for our convenient observation, interactions between shock and shock, shock and rarefaction, shock and contact surface, shock and subsonic region, and many others, all existing in their 'natural' state. Such interactions are the fundamental elements of most complex shock processes, and whatever understanding of them can be acquired from this source should aid in the comprehension of other involved processes in which they also participate.

In this survey we have included at least one example of every type of irregular pattern we have observed, and it now appears that extension of the study to other gas combinations would not produce any configurations fundamentally different from those shown here. Such an extension would not be without value, however, since the order of occurrence of the effects and the quantitative nature of the various separate interactions can be significantly varied by the proper choice of gases. In fact, it is this possibility of using different gas combinations that promises the necessary breadth of range for the use of irregular refraction patterns as display cases for aerodynamic interactions.

REFERENCES

BITONDO, D. 1950 Experiments on the amplification of a plane shock wave, Technical Report no. 7, Institute of Aerophysics, University of Toronto.

BLEAKNEY, W. & GRIFFITH, W. C. 1954 *Amer. J. Phys.* **22**, 597.

FLETCHER, C., TAUB, A. H. & BLEAKNEY, W. 1951 *Rev. Mod. Phys.* **23**, 271.

POLACHEK, H. & SEEGER, R. J. 1951 *Phys. Rev.* **84**, 922.

STONER, R. G., WOODBRIDGE, C. L. & DAVIES, E. B. 1952 Experimental observation of the interaction of shock waves at boundaries between various gases, Parts I and II, Pennsylvania State College Technical Report.

TAUB, A. H. 1947 Some numerical results on refraction of plane shocks, Technical Report II–1, Department of Physics, Princeton University.

TAUB, A. H. 1951 *Phys. Rev.* **72**, 51.